J. Fluid Mech. (1970), *vol.* 41, *part* 2, *pp.* 327–361
Boeing Symposium on Turbulence

The two-dimensional mixing region

By I. WYGNANSKI AND H. E. FIEDLER†
Boeing Scientific Research Laboratories, Seattle

(Received 1 June 1969)

The two-dimensional incompressible mixing layer was investigated by using constant-temperature, linearized hot wire anemometers. The measurements were divided into three categories: (1) the conventional average measurements; (2) time-average measurements in the turbulent and the non-turbulent zones; (3) ensemble average measurements conditioned to a specific location of the interface. The turbulent energy balance was constructed twice, once using the conventional results and again using the turbulent zone results. Some differences emerged between the two sets of results. It appears that the mixing region can be divided into two regions, one on the high velocity side which resembles the outer part of a wake and the other on the low velocity side which resembles a jet. The binding turbulent–non-turbulent interfaces seem to move independently of each other. There is a strong connexion between the instantaneous location of the interface and the axial velocity profile. Indeed the well known exponential mean velocity profile never actually exists at any given instant. In spite of the complexity of the flow the simple concepts of eddy viscosity and eddy diffusivity appear to be valid within the turbulent zone.

1. Introduction

The two-dimensional incompressible mixing region is considered as one of the 'simple' self preserving free shear flows. The turbulent structure of the flow was investigated by Liepmann & Laufer in 1947, and none of the investigations that followed were comparable in detail to this work. In most other cases the experiments were confined to the measurement of mean velocity. In attempting to make some comparisons between this flow and other free shear flows some major differences emerged. Most of these differences were attributed to the asymmetry of the two-dimensional mixing layer yet some were inexplicable on this basis. Since techniques of hot-wire anemometry have developed significantly over the last 20 years it seemed worthwhile to reconsider this flow. The investigation was not confined to a mere repetition of Liepmann & Laufer's work, but was extended to include third- and fourth-order products of the velocity fluctuations, spatial derivatives of these fluctuations, space-time correlations and intermittency. Furthermore, various zone average measurements were made, namely, an intermittency detecting network was constructed which, when coupled to an electronic switch, achieved the separation of the turbulent fluctua-

† Present address: Hermann-Föttinger-Institut fur Strömung technik Technische Universität Berlin.

Printed in Great Britain

tions inside the mixing region from the potential fluctuations outside the turbulent front. The importance of this discrimination was discussed by Kibens (1968) who showed that the intensity of the potential fluctuations outside the boundary layer may reach almost 40 % of their turbulent counterparts at a point where the intermittency factor γ is equal to 0·5. This finding raises the question whether the standard measurements adequately describe turbulent free shear flows.

The quantities measured were primarily aimed at the construction of energy balance, the study of which may shed most information on the problem. In constructing the energy balance an attempt was made to avoid as many assumptions as possible with regard to the flow structure.

Finally some velocity profiles conditioned to specific location of the interface were measured. Measurements of this type give some insight into the instantaneous picture of the flow which is apparently very different from whatever may be anticipated from knowledge of the average conditions.

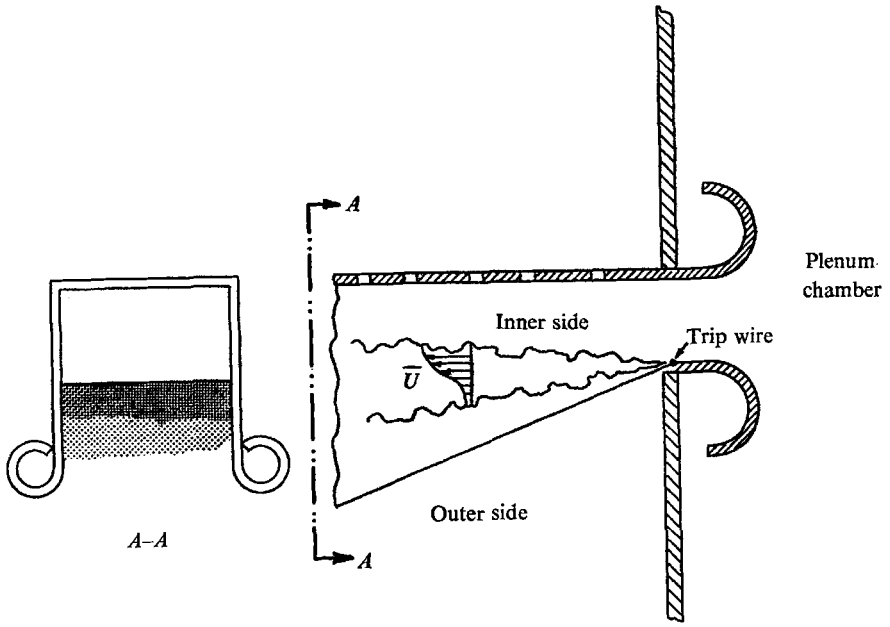

FIGURE 1. A schematic diagram of the test section.

2. The test facility and experimental method

A conventional blower-tunnel was used to supply the jet. A backward step blower powered by a 5 h.p. regulated direct current motor discharged into a plenum chamber 6 ft. in diameter. The plenum chamber was equipped with 3 screens and a deep honeycomb in order to reduce the turbulence level at the nozzle exist. The air was then discharged through a rectangular nozzle 7 in. wide and 20 in. long. The contraction ratio was 28 : 1 and the turbulence level was lower than 0·1 %.

The jet was allowed to mix on one of its boundaries with the surrounding

quiescent air (figure 1), the other 3 boundaries were solid. To prevent a lengthy transition region (6 cm in the case of Liepmann & Laufer (1947)) a trip wire was placed just upstream of the mixing region (figure 1). The air was cleaned using a Honeywell electrostatic precipitator and its temperature did not exceed the ambient room temperature by more than 1·5 °F. All measurements were made at a speed of 12 m/sec. Most of the measuring equipment and procedure was described in a previous paper (Wygnanski & Fiedler 1969).

Only the turbulent intensities were corrected for tangential cooling according to the formulae given by Champagne & Sleicher (1967). The response of the hot wire was assumed linear and no corrections resulting from higher order terms were applied. The higher order terms, which were measured, are presented in this paper.

All velocities are rendered dimensionless by dividing them by the free-stream velocity U_m. The origin of the lateral co-ordinate was chosen at a point at which the mean velocity was equal to one half its free-stream value and rendered dimensionless by dividing it by x, the distance from the hypothetical origin of the flow.

The various averages obtained in this investigation are defined as follows:

(1) The conventional average of any field variable $Q(t)$ is

$$\bar{Q} = \lim_{T\to\infty} \frac{1}{T}\int_0^T Q(t)\,dt.$$

(2) The turbulent zone average

$$\bar{Q}_T = \lim_{T\to\infty} \frac{1}{\gamma T}\int_0^T I(t)\,Q(t)\,dt,$$

where $I(t) = 1$ when the flow is turbulent, $I(t) = 0$ when the flow is potential, γ is the mean value of $I(t)$.

(3) The potential zone average

$$\bar{Q}_p = \lim_{T\to\infty} \frac{1}{(1-\gamma)T}\int_0^T [1-I(t)]\,Q(t)\,dt.$$

The turbulent and potential zone averages are related to the conventional average by

$$\bar{Q} = \bar{Q}_T\gamma + \bar{Q}_p(1-\gamma).$$

It is convenient to obtain the conventional square of the fluctuating component of a quantity by a capacitive coupling of the signal. Whenever it is desirable to obtain a zone average of a square of a fluctuating component the difference between the conventional d.c. level and the zone average d.c. level has to be taken into account. Thus the square of the quantity which is actually measured is

$$\begin{aligned}[Q(t)-\bar{Q}]^2 &= \{[Q(t)-\bar{Q}_T]+(\bar{Q}_T-\bar{Q})\}^2\\ &= [Q(t)-\bar{Q}_T]^2+(\bar{Q}_T-\bar{Q})^2+2[Q(t)-\bar{Q}_T](\bar{Q}_T-\bar{Q}),\end{aligned}$$

but the fluctuating quantity in the turbulent zone is given by $Q(t) = \bar{Q}_T + q_T$ and hence

$$[Q(t)-\bar{Q}]^2 = q_T^2+(\bar{Q}_T-\bar{Q})^2+2q_T(\bar{Q}_T-\bar{Q})$$

and $$\overline{[Q(t)-\bar{Q}]^2} = \overline{q_T^2} + (\bar{Q}_T - \bar{Q})^2.$$

Thus in order to obtain $\overline{q_T^2}$ the difference in the d.c. level should be known. The corrections become somewhat more involved when higher order zone-average cross-velocity products are to be obtained. The correction can either be applied analytically or in an analogue manner from d.c. power supply (Kibens 1968). In the present investigation the analytical method was used.

(4) One may also measure point averages which are conditioned to a specific location of the interface. In this case a distinction is made whether the detector probe enters ($\rightarrow$) or leaves ($\leftarrow$) the turbulent front. Thus if $\vec{I}(t) = 1$ when the probe enters the front and it is zero at all other times the leading edge point average is

$$\langle \vec{Q} \rangle = \lim_{n\to\infty} \frac{1}{n} \sum_{n=1}^{n} \vec{I}(tn) Q(tn),$$

where at an arbitrary time $t = 0$ the first leading edge of the turbulent front hits the detector probe. Similarly the trailing edge average

$$\langle \overleftarrow{Q} \rangle = \lim_{n\to\infty} \frac{1}{n} \sum_{n=1}^{n} \overleftarrow{I}(tn) Q(tn),$$

where $\overleftarrow{I}(t) = 1$ when the detector leaves the turbulent front and $\overleftarrow{I}(t) = 0$ at all other times.

The pulse time for which the integrating gate is open should be of course small in comparison with the time between successive pulses. The minimum number of samples required for a given accuracy is assessed from the frequency of crossing of the turbulent front, the pulse time, and the intensity of some turbulent fluctuations. In the present investigation only $\langle \overleftarrow{U} \rangle$ and $\langle \vec{U} \rangle$ were measured. The minimum number of samples taken was 5000 and the time of the individual pulse was 0·2 msec and 0·1 msec. A more detailed description of point averages and the acquisition times required are presented by Kibens (1968).

3. The intermittency factor

The basic signal used to distinguish between the turbulent and non-turbulent regions was $(\partial^2 u'/\partial t^2)^2 + (\partial u'/\partial t)^2$, the differentiating process eliminating the low frequency fluctuations which are associated with the potential flow. The addition of the two derivatives enabled a reduction in capacitive smoothing. The signal was processed in a manner similar to that suggested by Heskestad (1965); however, the triggering level did not have to be adjusted as the probe was moved from point to point. This fact was rather unusual since in most flows a continuous adjustment is necessary (e.g. Demetriades 1968, Wygnanski & Fiedler 1969). The Schmitt trigger signal was monitored and checked on a Tektronix dual-trace storage oscilloscope (figure 2). An attempt was made to process the signal $(\partial^2 u/\partial y\, \partial t)$ for the detection of turbulence (Kibens 1968) but the results were not superior to the above-mentioned signal.

Cumulative data of the spatial variation of the intermittency factor are shown in figure 3. It appears that stretches of irrotational flow exist throughout the mixing region. This is not a commonly observed fact but a similar observation was made by Hwang & Baldwin (1966) in the axisymmetric wake. Nevertheless,

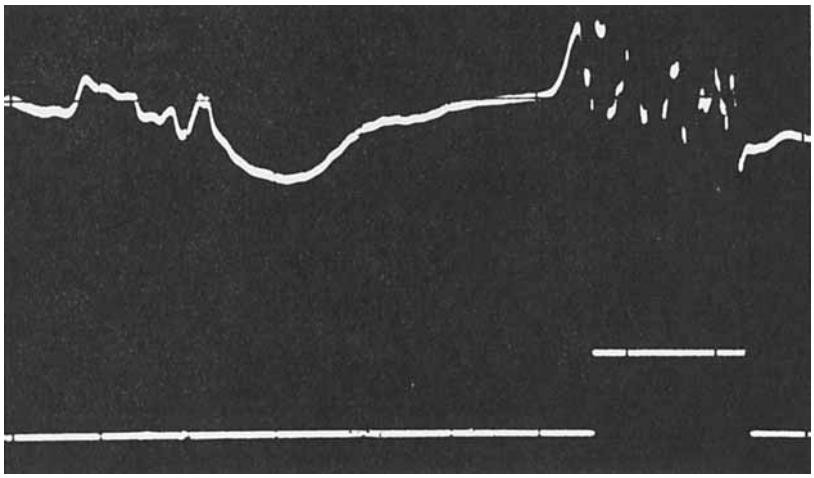

FIGURE 2. An oscillogram of the fluctuations of the longitudinal velocity component and the Schmitt trigger.

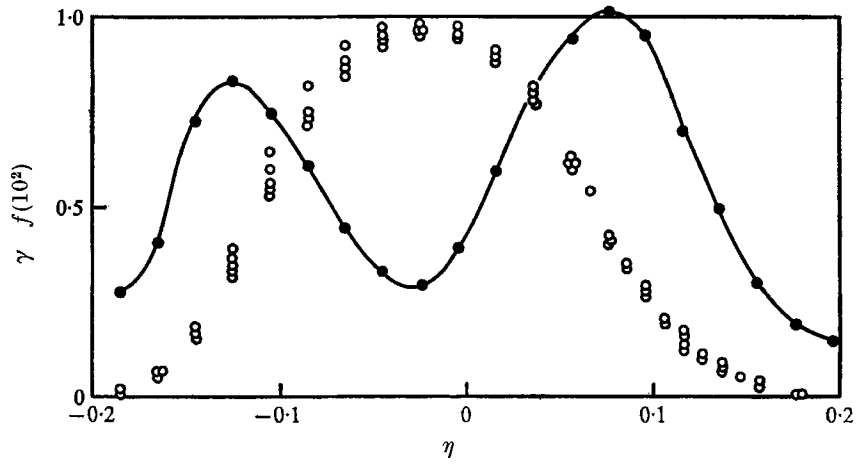

FIGURE 3. A cumulative distribution of intermittency and interface crossing rate. ○, γ; ●, f.

the curve shown in figure 3 is well approximated by two error functions as may be inferred from the probability plot of these results (figure 4). The average position of the turbulent front on the high velocity side of the flow is given by $\overline{\eta}_i = -0{\cdot}11$ while the corresponding position of the outer (low velocity) side of the flow is given by $\overline{\eta}_0 = 0{\cdot}07$. The standard deviations from these positions are $\sigma_i = 0{\cdot}036\eta$ on the inner side and $\sigma_0 = 0{\cdot}044\eta$ on the outer side. Since the value of

σ is associated with the large eddies, one may expect the integral scale on the low velocity side to be larger than on the high velocity side of the flow. From these observations it seems highly improbable that the excursions of the turbulent front on the high velocity side will ever reach the location where $\gamma_0 < 90\%$ and vice versa.

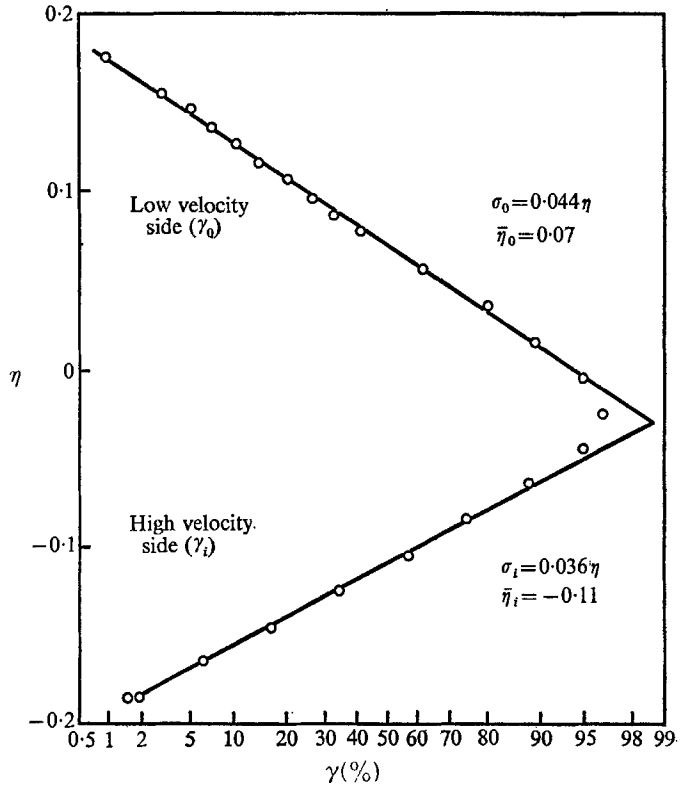

FIGURE 4. The distribution of intermittency drawn on probability paper.

The rate at which the turbulent front crosses a given point is also shown in figure 3. The curve has two peaks corresponding approximately in their location to $\gamma_0 = \gamma_i = 0{\cdot}5$. The maximum crossing rate of the inner turbulent front is approximately 80 $\sec^{-1}$ as compared with the crossing rate of 100 $\sec^{-1}$ of the turbulent front on the low velocity side. The average duration of a turbulent burst is γ/f and the average physical length of a burst may be obtained from the knowledge of the velocity at which the interface was convected downstream. The latter was not measured; however, the convection velocity of the large scale eddies was obtained from space time correlations of the filtered u' signal (figure 24). The two velocities should be essentially the same. Thus the length of a turbulent burst is given by $L_\gamma = (\gamma U_{\text{convection}})/f$. The ratio of σ/L_γ is a measure of the 'roughness' of the interface. Hence, at a location corresponding to $\gamma_i = 0{\cdot}5$, $\sigma_i/L_{\gamma i} = 0{\cdot}46$, and at a location corresponding to $\gamma_0 = 0{\cdot}5$, $\sigma_0/L_{\gamma_0} = 1{\cdot}83$. If instead of the convection velocity the velocity of the free stream (U_m) was used

the ratio of $\sigma/L_{\gamma i}$ would have been equal to 0·23. This number compares favourably with the corresponding value obtained by Kibens (1968) at the outer edge of the turbulent boundary layer. Indeed there are a number of similarities between the high velocity side of the mixing region at the outer part of a two-dimensional boundary layer or wake.

From the ratio $(\sigma^0/L_{\gamma 0})/(\sigma_i/L_{\gamma i}) \approx 4$, it may be concluded that the turbulent front is more flat on the high velocity side.

4. The mean velocity

The mean velocity was measured with a single hot-wire perpendicular to the uniform stream and with an X-wire. Both measurements yielded essentially the same results. The profile attained its similarity condition at $x = 12$ in. and even at $x = 8$ in. the velocity profile deviated very little from its fully developed form. The relatively short distance required for the mean flow to attain its

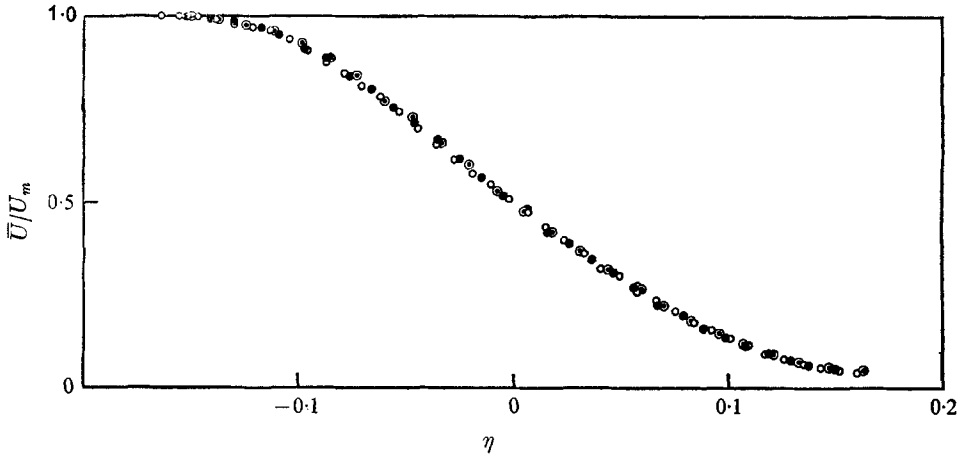

FIGURE 5. The conventional mean velocity profile. x: ○, 23·1 in.; ●, 19·23 in.; ⊙, 15·275 in.

equilibrium form is attributed in part to the trip wire which eliminated the initial transition region. The rate of spread of the flow is faster than the rate measured by Liepmann & Laufer (1947) and this fact may be attributed to the trip wire as well as to the presence of a solid surface in the plane $x = 0$ which were not used previously.† By choosing a spread parameter $\sigma = 9$ the present velocity profile becomes almost identical to that measured by Liepmann & Laufer. The velocity profile is shown in figure 5 and the locus of points at which the velocity is equal to $\frac{1}{2}$ the free-stream velocity is shown in figure 6. The mixing region thus grows linearly with downstream distance and the hypothetical origin of the flow is approximately $\frac{3}{4}$ in. upstream of the step. The averaging times required to obtain each point of the present data were much shorter than the corresponding

† The authors are indebted to a referee for this comment.

times in the axisymmetric self-preserving jet. It may be deduced from these figures that the turbulent flow spreads more rapidly on the quiescent side of the mixing region than on the high velocity side. The mean velocity in the turbulent zone, $\overline{U}_T$ is shown in figure 7 and the average potential velocity $\overline{U}_p$, between the turbulent bulges is shown on the same figure. Since γ is always less than unity, $\overline{U}_p$ is shown as a continuous curve although its value at the centre of the flow (where $\gamma > 90\,\%$) is somewhat doubtful. The free stream is decelerated between the turbulent bulges while the quiescent air is accelerated by the turbulent flow.

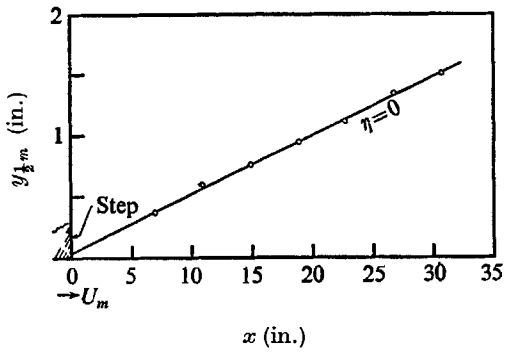

FIGURE 6. The growth of the mixing region with downstream distance.

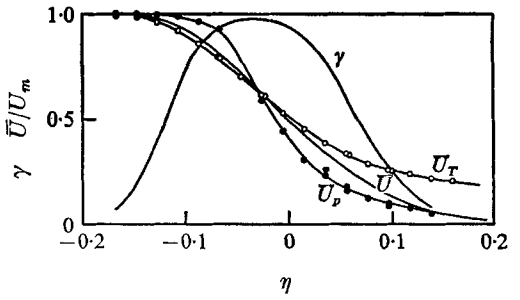

FIGURE 7. The distribution of the zone-average axial velocities. ○, $\overline{U}$ (turbulent); ●, $\overline{U}$ (potential).

The acceleration of the quiescent air is much more spectacular than the deceleration of the uniform stream. At the location corresponding to $\gamma_i = 0{\cdot}9$ the potential flow was decelerated to 95 % of the free-stream value while the outer fluid was accelerated to 32 % of the free-stream velocity at the corresponding location of $\gamma_0 = 0{\cdot}9$. The acceleration of the potential flow may be related to the 'roughness' of the interface σ/L_γ.

The conventional mean transverse velocity $\overline{V}$ as well as the zone averages of this velocity were measured and are shown in figure 4. However, the discussion of this figure is deferred to a later section in which the lateral energy transfer is discussed.

The point average velocities in the direction of streaming are shown in figures 8 and 9. The experimental results indicated that both leading-edge and trailing-edge point average velocities are identical. In one case the switch opens when the detector enters the turbulent front and the sample is taken when the detector is inside the turbulent region while in the other case the sample is taken after the detector left the turbulent zone. The relative shortness of the pulse-time relative to the time required for the 'bulge' to pass can explain this equality. The symmetry of the U velocity about the centre line of a turbulent 'bulge' was observed in the boundary layer (Kibens 1968).

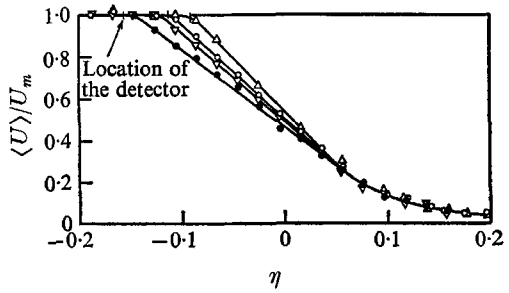

FIGURE 8. Some axial velocity profiles conditioned to a specific location of the turbulent interface on the high speed side of the flow. Intermittency at the detection station: ●, 0·1; ▽, 0·3; ○, 0·5; △, 0·7.

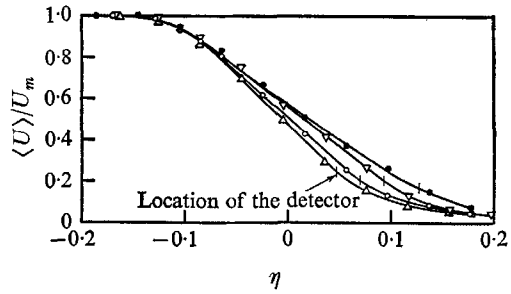

FIGURE 9. Some velocity profiles conditioned to a location of the interface on the low speed side of the flow. Intermittency at the detection station: ●, 0·1; ▽, 0·3; ○, 0·5; △, 0·7.

The velocity profiles conditioned to a given location of the interface on the inner side of the mixing region are shown in figure 8. Outside the detector probe the velocity is practically constant and equal to U_m. On the inner side of the probe the velocity profile drops linearly with distance from the detector. The linear dependence extends to $\eta \approx 0{\cdot}05$ (i.e. corresponding to $\gamma_0 \approx 0{\cdot}7$); further away from the detector all profiles coalesce to the conventional mean velocity profile. The weighted average of these profiles with the average frequency of the pulses at the detector yielded the conventional mean velocity profile. This fact may serve as an indirect check on the interface crossing rate measurement. A drastic change in $d\langle U\rangle/d\eta$ seems to occur over a very short distance across the

interface. Although $d\langle U\rangle/d\eta$ appears to be constant within the turbulent zone its value depends on the location of the interface. When the detector is moved to the low velocity side of the interface, very similar results are obtained except that now the velocity outside the interface continues to drop. The coalescing of the profiles on the far side from the interface which was monitored lead to the conclusion that each interface moves independently. Thus the mixing region as a whole does not flap like a flag about some average location. It seems plausible to infer that the instantaneous velocity profile in the turbulent region is approximately a straight line connecting U_m with $0{\cdot}2U_m$ over a lateral distance between the instantaneous locations of the two interfaces. The conventional mean velocity profile, $\overline{U}$, never exists in the flow, it is only the result of a long time averaging process over random excursions of the interfaces.

One may compare some of the present results on the high velocity side, with the measurements in the outer part of the boundary layer (Kibens 1968). The following conclusions may be drawn: (1) In both cases $\overline{U}_p$ is decelerated by approximately 5 % at $\gamma_i \approx 90\,\%$. (2) The zone average turbulent velocity $\overline{U}_T$ at $\gamma_i = 90\,\%$ is about $0{\cdot}82U_m$ while at the corresponding location in the boundary layer $\overline{U}_T = 0{\cdot}91U_m$. Hence the turbulent velocity gradient in the mixing region is significantly larger. (3) The point average velocity profiles within the turbulent region of the flow are in both cases linear functions of the lateral co-ordinate. However, whereas in the boundary layer the slope of the various profiles remains constant, in the mixing region $\partial\langle U\rangle/\partial\eta$ depends on the location of the interface and thus changes from profile to profile. These differences between the two flows may stem from the absence of a large region of fully turbulent fluid in the case of the mixing layer.

5. Fluctuation intensities and shear stress

In figures 10, 11 and 12 the r.m.s. values of the 3 components of velocity fluctuations are shown. All measurements were made with an X wire but some values of the longitudinal fluctuations were checked against an ordinary hot wire. The response of the wire was assumed linear and the direction of the mean flow was assumed to be parallel to the uniform stream. The results indicate that the flow is self preserving at $Re_x \approx 3 \times 10^5$ which is about 25 % smaller than the Reynolds number reported by Liepmann & Laufer (1947).

The maximum of $(\overline{u'^2})^{\frac{1}{2}}/U_m$ and $(\overline{v'^2})^{\frac{1}{2}}/U_m$ were 0·176 and 0·138 respectively. These intensities exceed the maxima measured by Liepmann & Laufer by about 10 % for u' and 25 % for v' fluctuations (when correction for tangential cooling is applied to both sets of data). The differences may again be attributed to the inadequately low frequency response to the old electronic networks (Wygnanski & Fiedler 1969).

The general shape of the curves is very similar in both investigations. It was also noticed that whereas the peak of $\overline{u'^2}$ fluctuations occurs at $\eta \approx 0$ the $\overline{v'^2}$ distribution has a peak at $\eta = -0{\cdot}045$ and the $\overline{w'^2}$ at $\eta = -0{\cdot}035$. The reason for the lateral shift between the peaks of $\overline{u'^2}$ and $\overline{v'^2}$ is not understood; how-

ever, this shift becomes even more evident whenever higher order terms are considered. In the central core of the mixing region the magnitude of $\overline{v'^2}$ is smaller than $\overline{w'^2}$ which in turn is smaller than $\overline{u'^2}$.

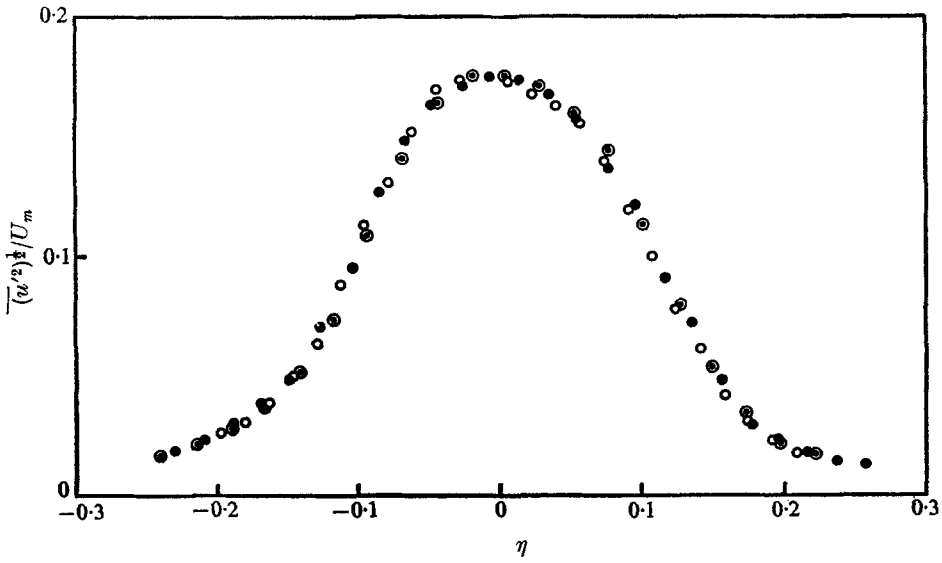

FIGURE 10. The conventional average distribution of the axial velocity fluctuations. x: ○, 23·725 in.; ●, 19·850 in.; ⊙, 15·900 in.

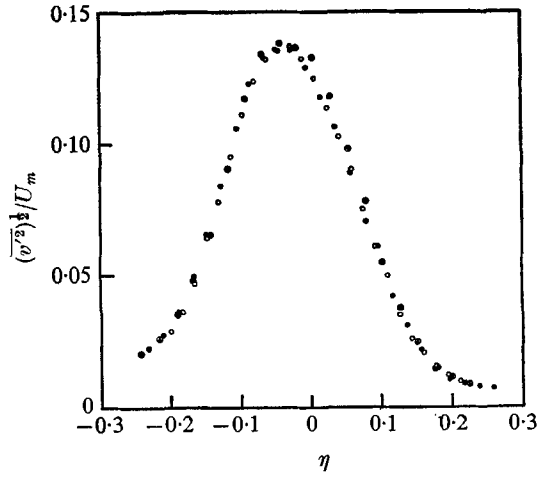

FIGURE 11. The conventional average distribution of the lateral velocity fluctuations. x: ○, 23·725 in.; ●, 19·850 in.; ⊙, 15·900 in.

The zone-average measurements of the three components of the velocity fluctuations are given in figures 13, 14 and 15 in which the conventional averages are shown as solid lines. The results presented were corrected for the d.c.-jump as indicated in §2. It is quite apparent from these figures that the intensities within the turbulent zone are highly inhomogeneous and

non-isotropic. The intensity of $(\overline{u'^2})_T$ is higher than the intensity of the other components in the outer (low velocity) and central regions of the flow. Only in the inner region ($\eta < -0{\cdot}1$) the intensities of $(\overline{v'^2})_T$ and $(\overline{w'^2})_T$ become larger than that of $(\overline{u'^2})_T$. The lateral shift in the location of the peak of the intensity

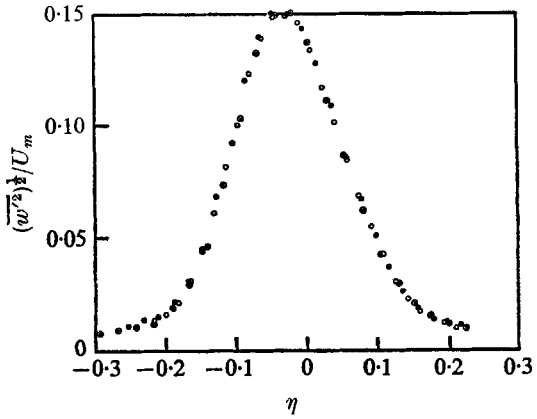

FIGURE 12. The conventional average distribution of the transverse velocity fluctuations. x: ○, 23·725 in.; ●, 19·850 in.; ⊙, 15·900 in.

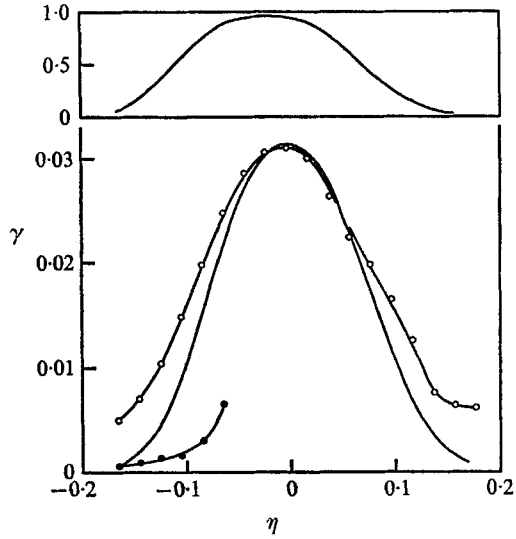

FIGURE 13. The zone average measurements of the longitudinal fluctuations. ——, $\overline{u'^2}/U_m^2$; ○, $(\overline{u'^2}/U_m^2)_T$; ●, $(\overline{u'^2}/U_m^2)_p$.

of the individual components in the turbulent zone remains. The distributions of $(\overline{u'^2})_T$ and $(\overline{w'^2})_T$ are more or less symmetrical about the peak, however the intensity of $(\overline{v'^2})_T$ drops rather slowly with decreasing η.

The intensity of the potential fluctuations is shown on the high velocity side of the flow only. The intensity of these fluctuations is not negligible when compared with the turbulent intensity even when they are weighted by γ.

For example at a location corresponding to $\gamma = 0{\cdot}5$, $(\overline{v'^2})_p \approx 0{\cdot}3(\overline{v'^2})_T$. Consequently very little can be inferred about the turbulent zone in a highly intermittent flow from the conventional measurements. A detailed discussion of this problem is given by Corrsin & Kistler (1955).

The theory of Phillips (1955) describing the potential fluctuations was previously compared with experimental results of Townsend (1951), Bradbury

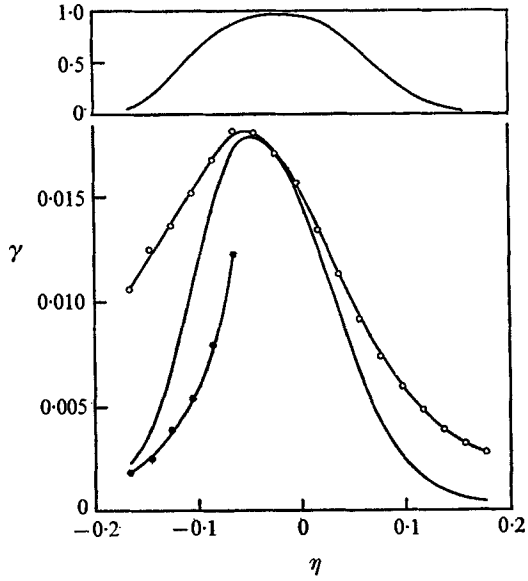

FIGURE 14. The zone average profiles of the lateral fluctuations.
——, $\overline{v'^2}/U_m^2$; ○, $(\overline{v'^2}/U_m^2)_T$; ●, $(\overline{v'^2}/U_m^2)_p$.

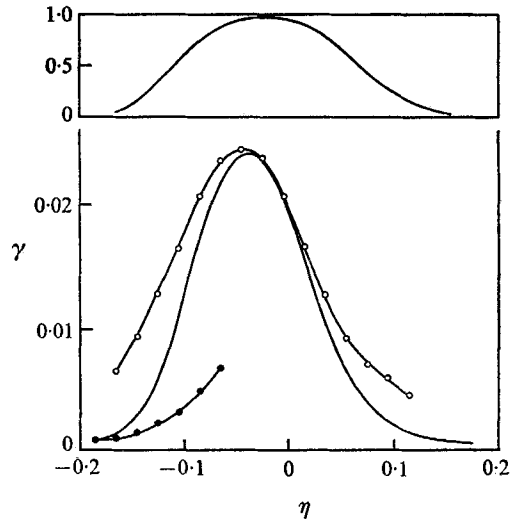

FIGURE 15. The zone average profiles of the transverse fluctuations.
——, $\overline{w'^2}/U_m^2$; ○, $(\overline{w'^2}/U_m^2)_T$; ●, $(\overline{w'^2}/U_m^2)_p$.

(1965), Bradshaw (1967) and Kibens (1968). In all cases with the exception of Kibens the measurements were made in a region where $\gamma \to 0$, i.e. quite far from the average position of the turbulent front. Since the squares of the potential fluctuations should asymptotically decay as y^{-4} (where y is a distance normal to the turbulent front and measured from some hypothetical origin) they become rapidly comparable to background turbulence level. Kibens has shown in the two-dimensional boundary layer that the asymptotic condition $(\overline{u'^2}) \propto y^{-4}$ applies even between the turbulent 'bulges' where the intensity is still quite

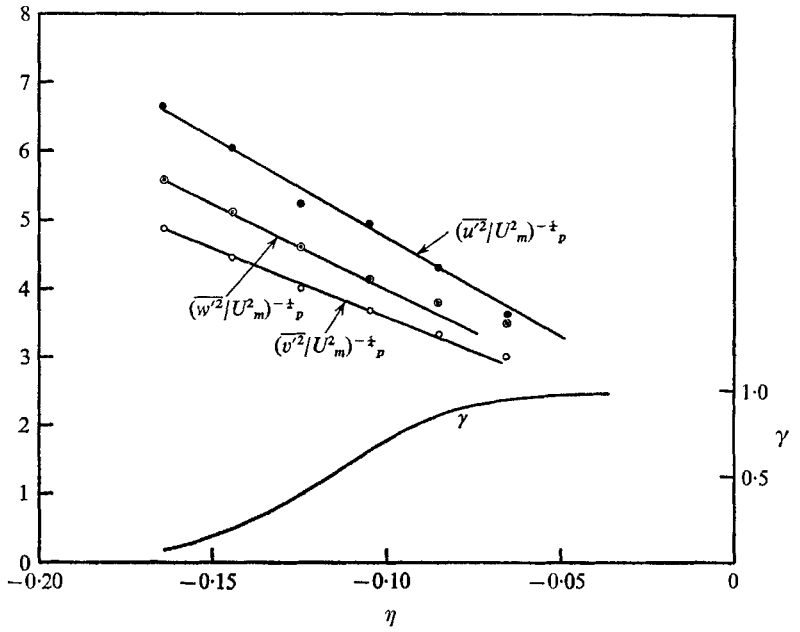

FIGURE 16. The potential fluctuations on the high velocity side of the flow.

η	$\left(\frac{\overline{u'^2}}{U^2_m}\right)_p$	$\left(\frac{\overline{w'^2}}{U^2_m}\right)_p$	$\left(\frac{\overline{u'^2}}{U^2_m}+\frac{\overline{w'^2}}{U^2_m}\right)_p$	$\left(\frac{\overline{v'^2}}{U^2_m}\right)_p$	$\left[\frac{\overline{v'^2}-(\overline{u'^2}+\overline{w'^2})}{\overline{v'^2}}\right]_p$
−0·165	0·000671	0·00105	0·00172	0·00180	4·4 %
−0·145	0·00099	0·00150	0·00249	0·00253	1·6 %
−0·125	0·00141	0·00230	0·00371	0·00392	4·84 %
−0·105	0·00161	0·00320	0·00481	0·00546	11·9 %
−0·085	0·00293	0·0050	0·00793	0·00794	0·13 %
−0·065	0·00625	0·00680	0·01305	0·0123	5·38 %

large. A more stringent test of the theory is to confirm the equation stating that $(\overline{u'^2})_p + (\overline{w'^2})_p = (\overline{v'^2})_p$ which is not limited to large values of y. This equation was confirmed as shown in figure 16. It is surprising that all components of the intensity of the potential fluctuations vary as y^{-4}, even at a distance equal to the mean position of the turbulent front.

On the low velocity side of the mixing region the large changes in the flow direction between the turbulent and non-turbulent zones and probably within the potential 'valleys' themselves pose a serious problem. Calculations based on the continuity equation indicate that the mean-flow direction in the turbulent

zone is essentially parallel to the uniform stream ($\tan^{-1}(\overline{V}/\overline{U})_T < 4°$). Calculations based on the conventional measurements indicate that at $\eta \approx 0{\cdot}12$, $\tan^{-1} \overline{V}/\overline{U} = 15°$ and increases rapidly with η, the estimates for the potential zone are much worse. Since the main purpose of the present investigation was to examine the turbulent field no effort was made to align the hot wire with the direction of the mean potential flow. Because of the angular misalignment with the mean flow, corrections should be applied to the conventional measurements for $\eta > 0{\cdot}1$. These corrections arise from the failure of the cosine law (tangential cooling) and the interference of the stem. For this reason the intensity of the potential fluctuations on the outer side of the flow is not shown.

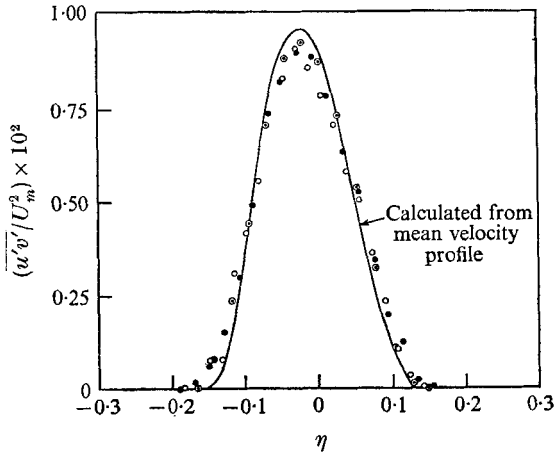

FIGURE 17. The conventional average shear stress distribution.
x: ○, 23·725 in.; ●, 19·800 in.; ⊙, 15·900 in.

The conventional average distribution of the shear stress is shown in figure 17. The solid curve on the same figure shows the distribution of shear stress as calculated from the mean velocity profile. The calculation proceeded from the high velocity side and proved to be independent of the location at which the boundary conditions were applied, provided that location was chosen sufficiently far away from the mixing zone so that $\overline{U}/U_m = 1$ and $d(\overline{U}/U_m)/d\eta = 0$. The location at which $\overline{u'v'}$ is maximum corresponds to the location at which $d^2(\overline{U}/U_m)/d\eta^2 = 0$ and there was no necessity to impose that condition as a boundary condition (see Liepmann & Laufer 1947). The fact that the measured and calculated shear stress distributions agree quite well is attributed to the small scatter in the mean velocity profile.

The zone average distribution of $\overline{u'v'}$ is given in figure 18. The profile of $(\overline{u'v'})_T$ is not symmetrically distributed about the conventional mean profile. While $(\overline{u'v'})_T$ is almost constant on the outer part of the flow it drops quickly on the high velocity side. Very little can be said about $(\overline{u'v'})_p$ except that it is very small and indeed may be non-existent; on the low velocity side of the flow even negative values of $(\overline{u'v'})_p$ were measured and were also estimated from the other $\overline{u'v'}$ measurements.

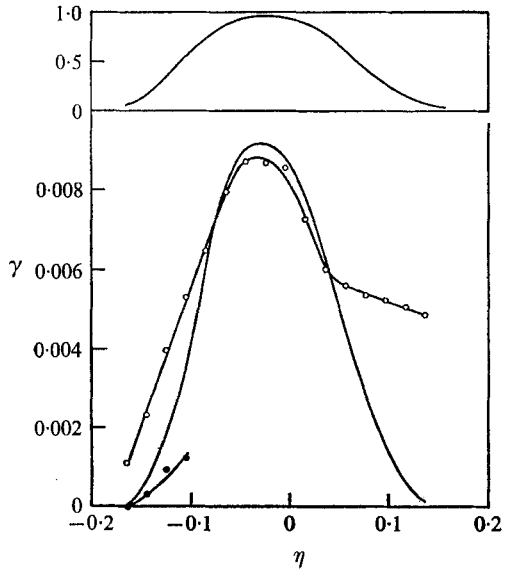

FIGURE 18. The zone average measurements of shear stress. ——, $\overline{u'v'}/U_m^2$; ○, $(\overline{u'v'}/\overline{U_m^2})_T$; ●, $(\overline{u'v'}/\overline{U_m^2})_p$.

6. Correlations and spectra

Two point space-time correlations were measured along the line $\eta = 0$ at various distances from the origin. Measurements across the flow were done at a single section corresponding to $x = 19{\cdot}47$ in. Providing the flow is self preserving the results of these measurements should be applicable to any other point in the flow. The R_{11} correlation was measured by keeping one probe stationary and moving the other one in the downstream direction; for the R_{12} correlation both probes were moved an equal lateral distance about the point at which the correlation distribution was to be measured.

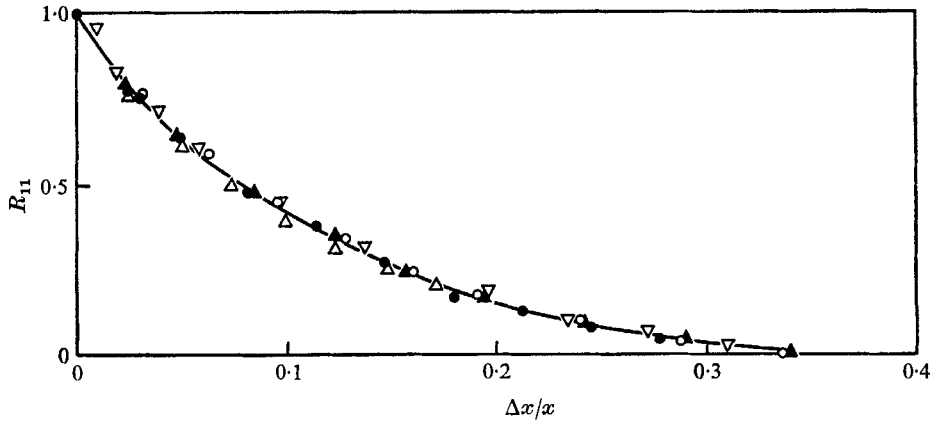

FIGURE 19. Longitudinal correlation at the centre of the flow ($\eta = 0$). ○, 11·54 in.; ▲, 15·50 in.; ▽, 19·47 in.; ●, 23·35 in.; △, 31·35 in. $(L_x)_{\overline{U}=0{\cdot}5U_m} = 0{\cdot}1025x$.

In figure 19 the R_{11} correlation at $\eta = 0$ and various cross sections is plotted *vs.* $\Delta x/x$. The results collapsed on a single curve indicate the existence of self preservation as far as the various scales are concerned. The integral scale obtained from this figure is $(L_x)_{\eta=0} = 0{\cdot}1025x$. The integral scale may also be obtained from the spectral measurements of the energy containing eddies by using the equation

$$L_x = \frac{\pi}{2}\frac{E_1(0)}{\overline{u'^2}}.$$

From figure 26 one may calculate that $(L_x)_{\eta=0} = 0{\cdot}104 \cdot x$ which differs by less than 2 % from the L_x obtained by integrating the correlation measurement.

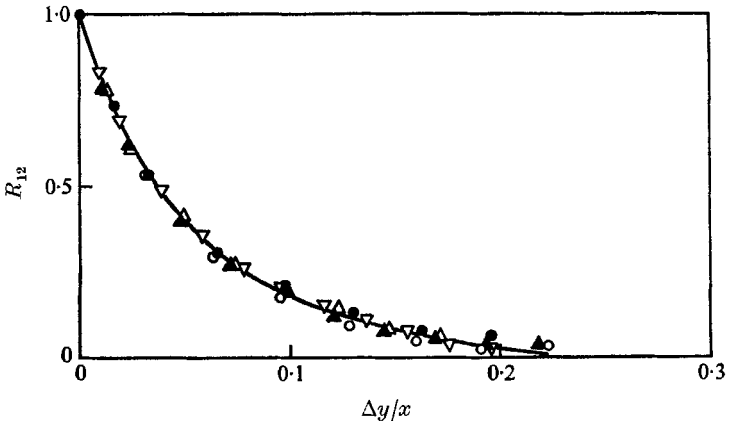

FIGURE 20. Lateral correlation at the centre of the flow ($\eta = 0$). ○, 11·54 in.; ▲, 15·50 in.; ▽, 19·47 in.; ●, 23·35 in.; △, 31·35 in. $(L_y)_{\overline{U}=0{\cdot}5U_m} = 0{\cdot}0555x$.

In figure 20 the R_{12} correlation is plotted *vs.* $\Delta y/x$ and similar conclusions regarding self preservation may be drawn from it. The dimensionless correlation coefficients appear to attain their self-preserving distribution at a distance, x, which is smaller than the distance required by the intensity to reach its self-preserving level. This fact may also be inferred from the measurements in the axisymmetric jet (Wygnanski & Fiedler 1969).

A lateral traverse of R_{11} and R_{12} correlations (figures 21 and 22) indicates an increase in integral scales towards the outer part of the flow. The variation of scales is not a continuous ever increasing function of η, as it is in the axisymmetrical jet, but rather a step function dividing the flow into two quite distinct regions. In each of the above-mentioned regions the integral scale is approximately constant. In the inner region $(L_y)_i \approx 0{\cdot}0364x$ and $(L_x)_i \approx 0{\cdot}098x$ while in the outer region $(L_y)_0 \approx 0{\cdot}0575x$... and $(L_x)_0 \approx 0{\cdot}147x$. The division into two regions is more apparent in the R_{12} correlation distribution than in R_{11}. In the former case the inner region corresponds to the zone in which $\gamma_i < 0{\cdot}9$ and the outer region extends inwards to an η corresponding to $\gamma_0 < 0{\cdot}9$; the transition from one integral scale to another occurs at values of η corresponding to $\gamma > 0{\cdot}9$. The results are not as clear in the R_{11} distribution because the distance, Δx, between the two sensors is measured parallel to the uniform stream, while

the flow diverges with x. Some comparison may be made with the findings in the axisymmetric mixing layer, which should exhibit similar characteristics although it is not a truly self-preserving flow. According to Laurence (1956) L_y remains constant across the flow; however, according to Bradshaw *et al.* (1963), L_y increases with increasing outward distance. These observations may

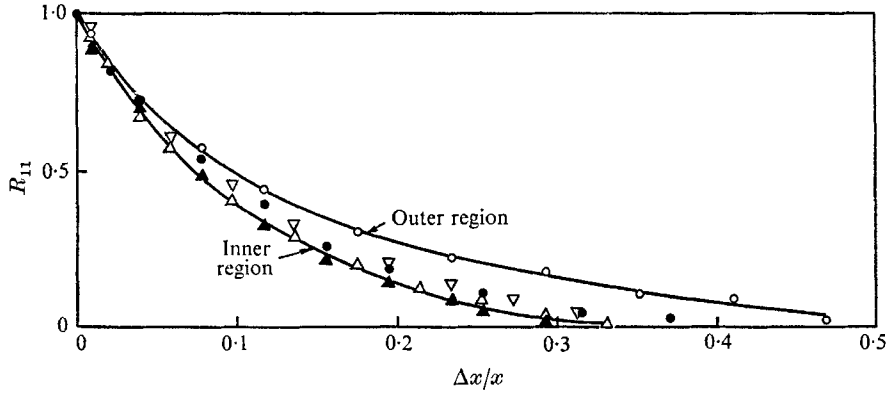

FIGURE 21. Variation of longitudinal correlations across the mixing region. η: ●, −0·145; △, −0·105; ▲, −0·045; ▽, 0·0165; ○, 0·0770. $(L_x)_i = 0{\cdot}0982x$, $(L_x)_0 = 0{\cdot}147x$.

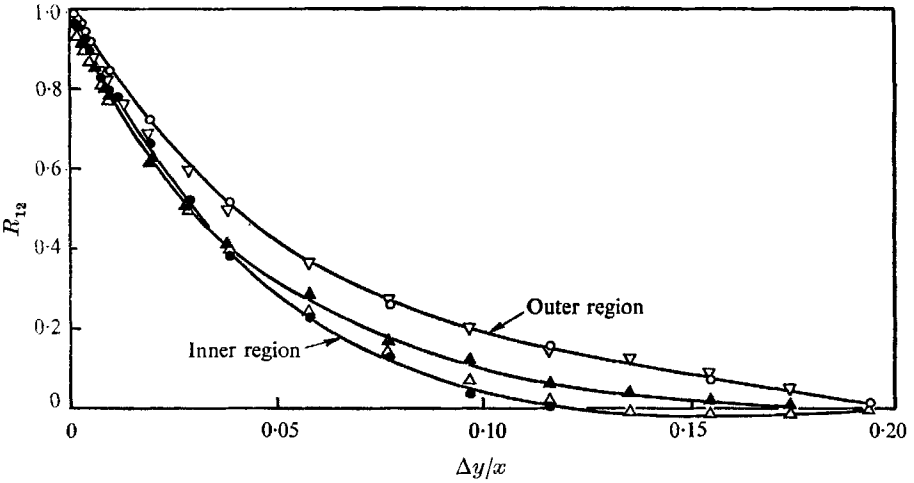

FIGURE 22. The distribution of lateral correlations across the mixing region. η: ○, 0·0770; ▽, 0·0165; ▲, 0·035; △, 0·105; ●, 0·145. $(L_y)_i = 0{\cdot}0364x$, $(L_y)_0 = 0{\cdot}0575x$.

not be in conflict as one assumes that the first was based on measurements within a single region while the second was deduced from too few measurements made across the entire flow. The integral scale observed by Laurence was given by $L_y = 0{\cdot}036x$ which agrees with the present measurements on the high velocity side of the flow.

The lateral integral scales in wakes (L_y) are generally larger than in jets (Bradbury 1965). Consequently the present behaviour of L_y is contrary to the

assumption that the results in the wake and the jet may be superimposed to represent the two-dimensional mixing layer.

The convection velocity of the energy containing eddies was obtained from the cross-correlations of the u' signal as shown by Davies *et al.* (1963). The convection velocity of the small eddies was obtained in the same manner but using $(\partial u'/\partial t)$ instead (figure 23). The dissipation scales are convected downstream at a larger velocity than the energy containing eddies; this velocity is generally larger than the local mean velocity except near the inner edge of the mixing region, where $\overline{U}_c$ (of $\partial u'/\partial t$) $= 0{\cdot}97U_m$. The convection velocity of the energy containing eddies is slower and is approximately equal to $0{\cdot}85U_m$ at the inner edge of the flow. Near the core region of an axisymmetric jet $\overline{U}_c \approx 0{\cdot}65U_m$ and it varies more slowly with radial distance than the mean velocity (Davies *et al.* 1963). In the fully developed region of the axisymmetric jet $\overline{U}_c \approx U_m$ on the centre line but $d\overline{U}_c/d\eta < d\overline{U}/d\eta$ so that in the outer region of the flow $\overline{U}_c > \overline{U}$ (Wygnanski & Fiedler 1969). In the present flow $d\overline{U}_c/d\eta$ is larger than in the axisymmetric configuration so that $\overline{U}_c$ does not exceed $\overline{U}$ at any point in the flow. The relatively large value of $d\overline{U}_c/d\eta$ may be associated with a lack of large-scale eddies which extend across the entire flow.

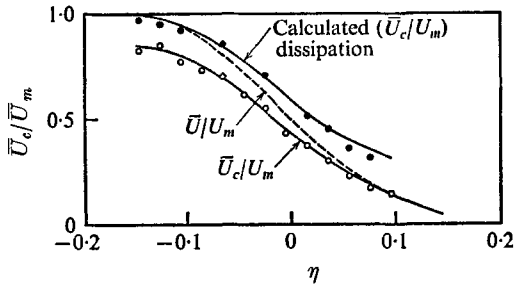

FIGURE 23. The variation of convection velocities across the flow. ●, measured values from $\partial u'/\partial t$ signal.

Heskestad (1965) suggested a transformation from temporal to spatial derivatives which accounts for relatively high turbulence levels. The derivation embodies the assumptions of isotropy and the independence of the large-scale eddies and the small-scale eddies. The transformation for a normal hot wire in the x, y plane is given by

$$\left(\overline{\frac{du'}{dt}}\right)^2 \Big/ \left(\overline{\frac{du'}{dx}}\right)^2 = \overline{U}^2\left[1+\frac{\overline{u'^2}}{\overline{U}^2}+2\frac{\overline{v'^2}}{\overline{U}^2}+\frac{\overline{w'^2}}{\overline{U}^2}\right].$$

This equation defines the convection velocity of the dissipative eddies and may be compared with experimental results. Since we are interested in the small-scale motion it is appropriate to use the turbulent zone averages for this purpose; hence

$$\left(\frac{\overline{U}_c}{U_m}\right)_{\text{dissipation}} = \left[\left(\frac{\overline{U}}{U_m}\right)_T^2+\left(\frac{\overline{u'^2}}{U_m^2}\right)_T+2\left(\frac{\overline{v'^2}}{U_m^2}\right)_T+\left(\frac{\overline{w'^2}}{U_m^2}\right)_T\right]^{\frac{1}{2}}.$$

This equation is presented in figure 23. The agreement between the predicted convection velocity and the observed one is quite good except at the edges of the

flow. Although Heskestad's derivation includes a number of gross assumptions, some of which do not apply to the present flow (e.g. the isotropic relations among the derivatives), the usefulness of the final result is apparent.

The convection velocity of the filtered signal is shown in figure 24. The measurements were done at three points across the flow. The graphs indicate that the larger eddies travel slower but there is no significant increase in convection velocity at the high frequencies as was observed in the axisymmetric jet.

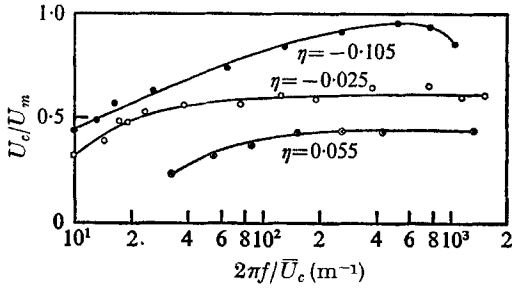

FIGURE 24. The wave-number dependence of the convection velocity.

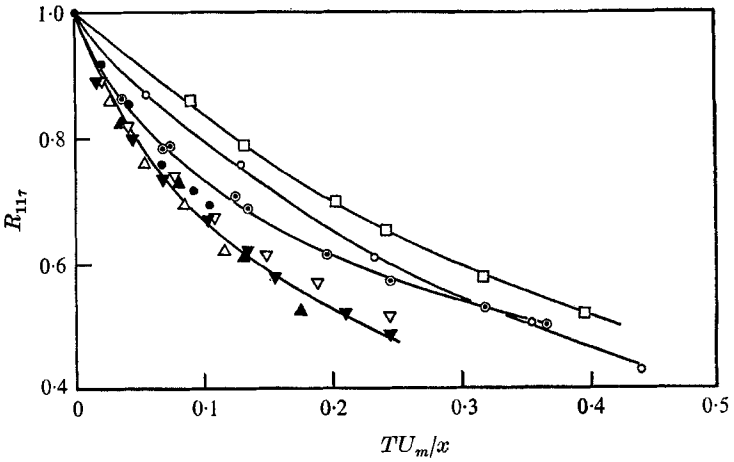

FIGURE 25. The distribution of the $R_{11\tau}$ correlations in the moving frame of reference across the mixing region. η: ●, −0·125; ▲, −0·105; △, −0·085; ▼, −0·045; ▽, −0·024; ⊙, 0·036; ○, 0·077; □, 0·096.

The fact that only the two upper curves tend to coalesce at the low-frequency end serves as additional evidence that the large-scale eddies do not extend across the entire flow.

The moving frame auto-correlations are plotted in figure 25 for various locations in the mixing region. Since the correlation coefficient does not go below 0·5 one cannot determine the associated integral time scales by direct integration. One may proceed in the manner outlined by Davies *et al.* and fit an exponential curve to these measurements. But even without doing so it is again obvious (see Wygnanski & Fiedler 1969) that no simple relationship between the integral time scale and mean shear exists.

The power spectral densities of the energy containing eddies are shown in figure 26. The percentage of the turbulent energy present at the very low-frequency-end of the spectrum (below 5 cps) is significantly less than in the axisymmetric jet. This is reflected in somewhat shorter integration times required to obtain the measurements. Although the same equipment was used in both investigations, little attention had to be paid to frequencies lower than 1 cps in the present case. The spectral measurements were carried to frequencies as low as 0·2 cps (the corresponding wave-number is 0·25 m^{-1}) but they did not show any discontinuity which may point to a distinct two-component structure, as observed by Townsend (1950) in the self-preserving wake.

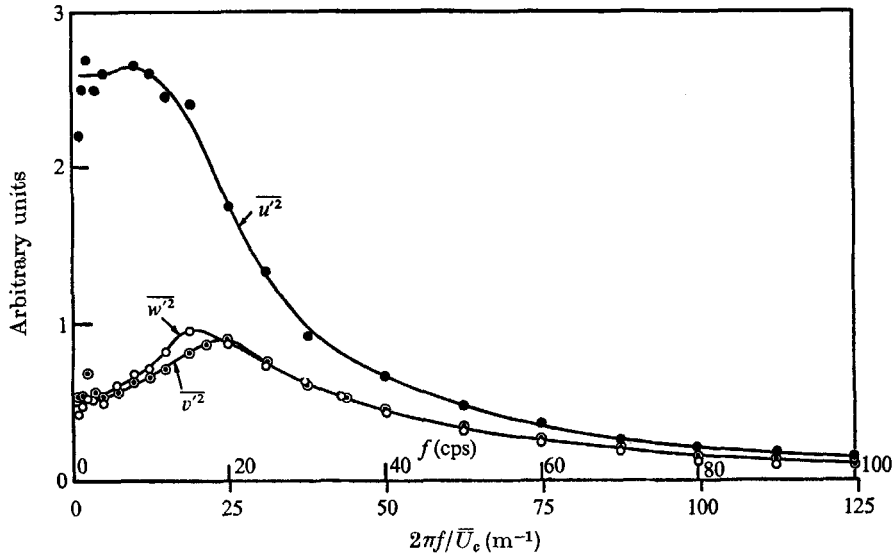

FIGURE 26. One dimensional spectra of the energy containing eddies. (Location $x = 19{\cdot}47$ in., $\eta = 0$.)

7. Higher order velocity products

The knowledge of triple velocity products is necessary to evaluate the diffusion term in the energy balance and to correct lower order products. The measurements were made at a distance of 19·47 in. from the step and are presented in figures 27 to 33. The experimental procedure used is described with the measurements in the axisymmetrical jet (Wygnanski & Fiedler 1968).

The conventional-average measurements and the turbulent-zone-average measurements of the cross-products are shown in figures 27 and 28. All quantities are of the same order of magnitude and there is no appreciable difference between the two averaging processes. The only difference worth mentioning is that $(\overline{u'v'^2})_T$ and $(\overline{v'u'^2})_T$ become negative at the outer edge of the flow, while the conventional measurements indicate that they simply tend to zero.

The distributions of $\overline{u'^3}$ and $\overline{v'^3}$ are shown in figure 29. The difference between the conventional average and the zone average results is quite dramatic. Whereas the conventional results decrease smoothly to zero at the edges, $(\overline{u'^3})_T$ keeps

increasing towards the low velocity side of the flow and the absolute value of $(\overline{v'^3})_T$ keeps increasing on the high velocity side of the flow. In addition $(\overline{u'^3})_T$ is an order of magnitude larger than all other quantities (it is multiplied only by 10^2). The results were consistently repeatable and they indicate that the

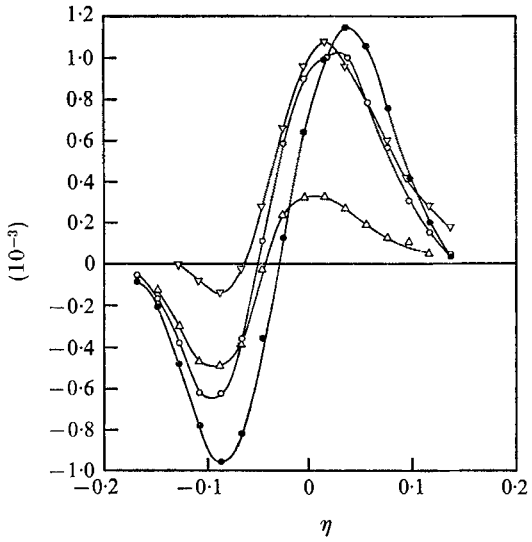

FIGURE 27. The distribution of conventional third-order cross products. ●, $\overline{v'u'^2}/U_m^3$; △, $\overline{v'w'^2}/U_m^3$; ▽, $\overline{u'w'^2}/U_m^3$; ○, $\overline{u'v'^2}/U_m^3$.

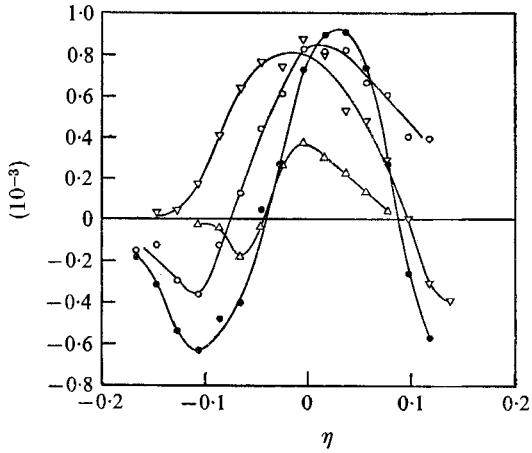

FIGURE 28. The distribution of third-order cross products in the turbulent zone. ●, $(\overline{v'u'^2}/U_m^3)_T$; △, $(\overline{v'w'^2}/U_m^3)_T$; ▽, $(\overline{u'w'^2}/U_m^3)_T$; ○, $(\overline{u'v'^2}/U_m^3)_T$.

diffusion process is different on the two sides of the flow. In constructing the turbulent energy balance it is customary to neglect the term associated with $\overline{u'q^2}$ by introducing the boundary-layer approximation. In view of the large magnitude of $(\overline{u'^3})_T$ such simplification is erroneous.

The skewness factors of the conventional measurements are shown in figure 30. Although these results can be deduced from the previously presented figures they are shown here as they exhibit the same tendencies as the plots of $(\overline{u'^3})_T$ and $(\overline{v'^3})_T$. The skewness factor of the w' signal is shown on this figure as well. The values of $\overline{w'^3}/U_m^3$ are an order of magnitude smaller than $\overline{v'^3}/U_m^3$ and never exceeded 2×10^{-4}. The increase in $\overline{w'^3}/(\overline{w'^2})^{\frac{3}{2}}$ towards the outer edge results primarily from the decrease of $\overline{w'^2}$ in that region and is in part attributed to uncertainties in the mean flow direction. The skewness factors of the x-derivatives of the respective components of the fluctuations are shown in figure 31.

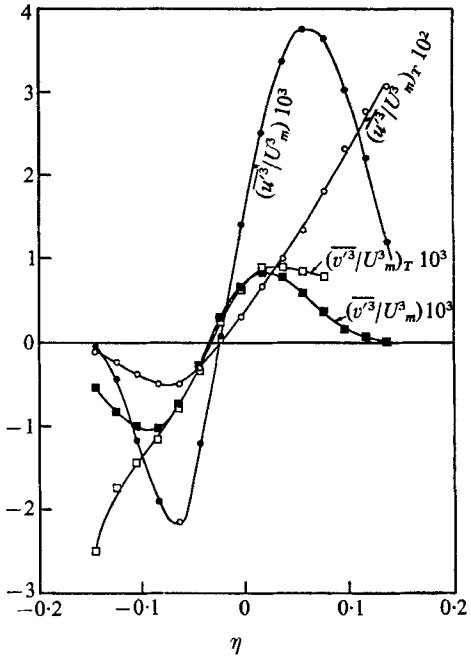

FIGURE 29. The third-order products—turbulent zone and conventional averages.

The flatness factors of the fluctuations and their derivatives were used by Townsend to detect intermittency on the assumption that

$$\gamma = \frac{\text{flatness factor on centre line}}{\text{local flatness factor}}.$$

The results in the wake (Townsend 1949*a*) and in the turbulent boundary layer (Townsend 1951) are quite consistent in spite of their scatter. The intermittency based on this assumption in jets appeared to disagree with the measured results of Heskestad (1965) and Wygnanski & Fiedler (1969).

In figures 32 and 33 the flatness factors of the fluctuations and their derivatives are shown. The intermittency distribution derived from the flatness factor of the fluctuations is too wide in comparison with the measured γ particularly at the edges of the flow. This may be attributed in part to the potential fluctuations and the large-scale motion within the turbulent front. On the other

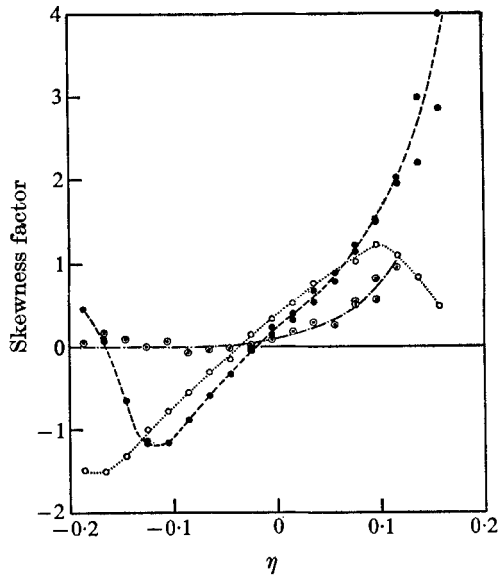

FIGURE 30. The distribution of skewness factors across the flow. --●--, $\overline{u'^3}/(\overline{u'^2})^{\frac{3}{2}}$; ····○····, $\overline{v'^3}/(\overline{v'^2})^{\frac{3}{2}}$; —·—⊙—·—, $\overline{w'^3}/(\overline{w'^2})^{\frac{3}{2}}$.

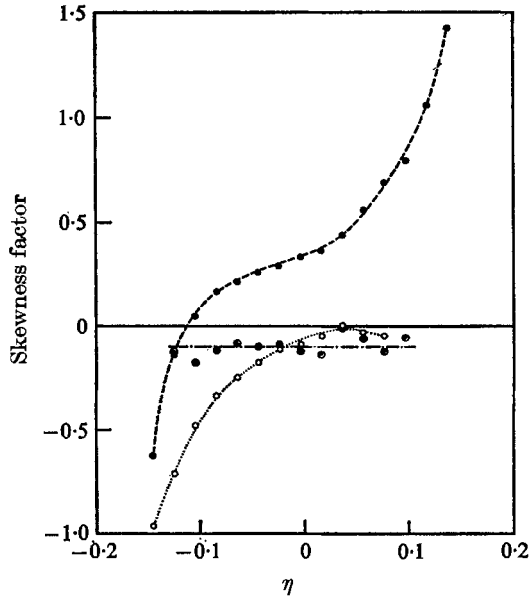

FIGURE 31. The skewness factors of the derivative signal.

--●--, $\overline{\left(\frac{\partial u'}{\partial x}\right)^3}\Big/\left[\overline{\left(\frac{\partial u'}{\partial x}\right)^2}\right]^{\frac{3}{2}}$; ···○···, $\overline{\left(\frac{\partial v'}{\partial x}\right)^3}\Big/\left[\overline{\left(\frac{\partial v'}{\partial x}\right)^2}\right]^{\frac{3}{2}}$;

—·—⊙—·—, $\overline{\left(\frac{\partial w'}{\partial x}\right)^3}\Big/\left[\overline{\left(\frac{\partial w'}{\partial x}\right)^2}\right]^{\frac{3}{2}}$.

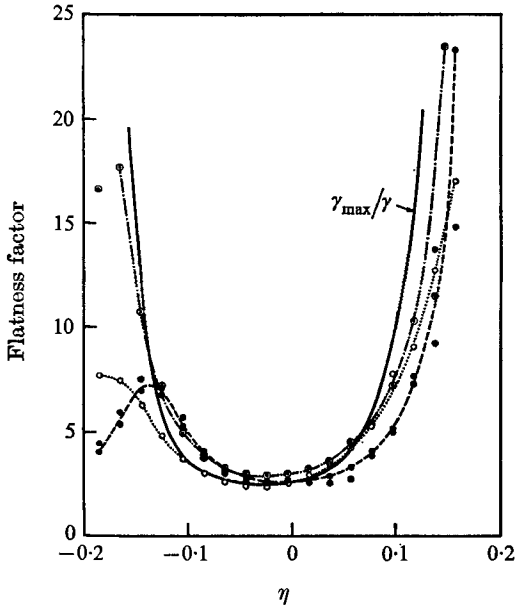

FIGURE 32. The distribution of conventional flatness factors.
--●--, $\overline{u'^4}/(\overline{u'^2})^2$; ···○···, $\overline{v'^4}/(\overline{v'^2})^2$; —·—⊙—·—, $\overline{w'^4}/(\overline{w'^2})^2$.

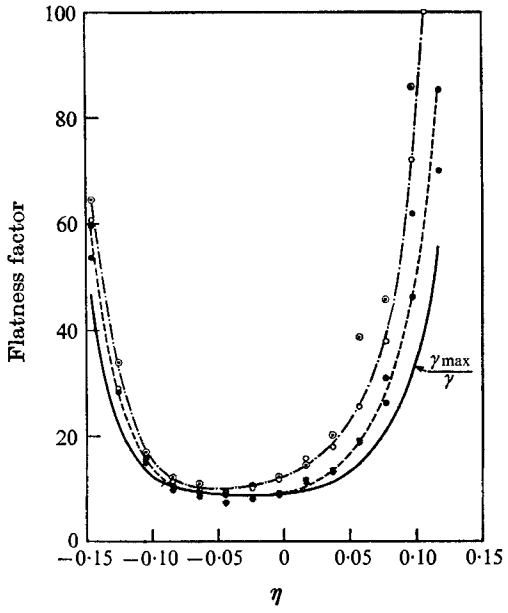

FIGURE 33. The conventional flatness factors of the derivative signal.
--●--, $\overline{\left(\frac{\partial u'}{\partial x}\right)^4}\Big/\left[\overline{\left(\frac{\partial u'}{\partial x}\right)^2}\right]^2$; —·—○—·—, $\overline{\left(\frac{\partial v'}{\partial x}\right)^4}\Big/\left[\overline{\left(\frac{\partial v'}{\partial x}\right)^2}\right]^2$;
—·—⊙—·—, $\overline{\left(\frac{\partial w'}{\partial x}\right)^4}\Big/\left[\overline{\left(\frac{\partial w'}{\partial x}\right)^2}\right]^2$.

hand the profile of intermittency derived from the differentiated signal is too narrow as it accentuates the dissipation scales. The two curves together may, of course, give the required average results if one accepts the inevitable scatter.

8. The dissipation terms and microscales

Five out of the nine derivatives composing the dissipation term have been measured. Three temporal derivatives were transformed to spatial derivatives in the x direction *via* the convection velocity of the $\partial u'/\partial t$ signal. Two transverse derivatives were measured by subtracting the signals of two parallel wires which were set 0·2 mm apart. The conventional and turbulent-zone averages are shown in figures 34 and 35. The ensuing γ_f and λ_g microscales are shown in figures 36 and 37 where figure 37 represents the growth of λ_f with the distance from the step along the line $\eta = 0$.

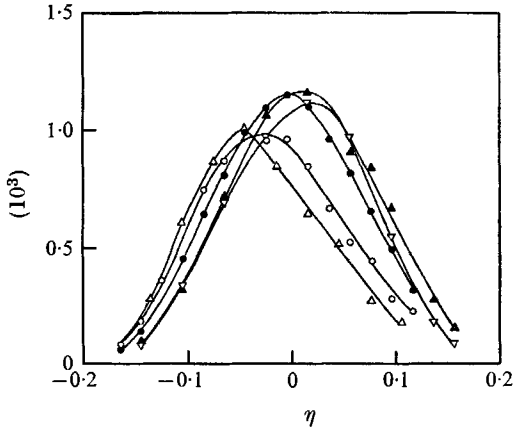

FIGURE 34. The measured dissipations terms.

▲, $\left(\overline{\frac{\partial u'}{\partial y}}\right)^2 \cdot \frac{x^2}{U_m^2}$; ▽, $\left(\overline{\frac{\partial u'}{\partial z}}\right)^2 \cdot \frac{x^2}{U_m^2}$; ●, $\left(\overline{\frac{\partial u'}{\partial x}}\right)^2 \cdot \frac{x^2}{U_m^2}$; ○, $\left(\overline{\frac{\partial v'}{\partial x}}\right)^2 \cdot \frac{x^2}{U_m^2}$; △, $\left(\overline{\frac{\partial w'}{\partial x}}\right)^2 \cdot \frac{x^2}{U_m^2}$.

The conventional measurements indicate that all terms have approximately the same distribution across the flow and are equal in magnitude. Thus it may be inferred that the flow is not isotropic. It was initially believed that the potential fluctuations affect the results and the turbulent zone averages would conform with the isotropic relations. This expectation did not materialize because all derivatives of the longitudinal fluctuations in the turbulent zone are again approximately equal and increase almost linearly with η. On the low velocity side not only $\overline{(\partial u'/\partial x)^2} \neq \frac{1}{2}\overline{(\partial v'/\partial x)^2}$ but it is almost double $\overline{(\partial v'/\partial x)^2}$.

It was observed previously (e.g. Klebanoff 1955) that the derivatives did not obey the isotropic relations, but the disagreement cannot indicate whether the anisotropy exists at other wave-numbers as well. One, of course, does not expect isotropy to exist at the very low wave-numbers which are directly related to the mean shear (see also figure 26).

The microscales measured in the turbulent zone are smaller than those obtained by conventional measurements. The difference between the two types of measurement is particularly significant at the edges of the flow where the potential fluctuations are important. The microscales do not vary much across the flow but they slowly increase with downstream distance. The variation of λ_f with x is essentially linear; however, λ_f does not equal zero at the origin of the flow. Some attempts were made to obtain the microscales from correlation measurements but the results were not satisfactory.

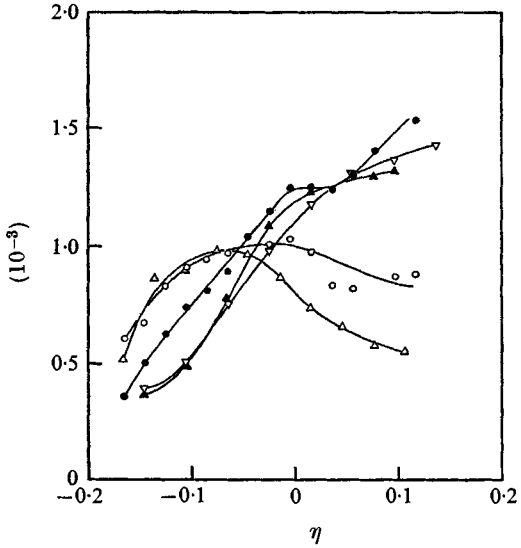

FIGURE 35. The dissipation terms in the turbulent zone.
●, $\left(\overline{\frac{\partial u'}{\partial x}}\right)^2_T \cdot \frac{x^2}{U_m^2}$; ○, $\left(\overline{\frac{\partial v'}{\partial x_i}}\right)^2_T \cdot \frac{x^2}{U_m^2}$; △, $\left(\overline{\frac{\partial w'}{\partial x}}\right)^2_T \cdot \frac{x^2}{U_m^2}$; ▽, $\left(\overline{\frac{\partial u'}{\partial z}}\right)^2_T \cdot \frac{x^2}{U_m^2}$; ▲, $\left(\overline{\frac{\partial u'}{\partial y}}\right)^2_T \cdot \frac{x^2}{U_m^2}$.

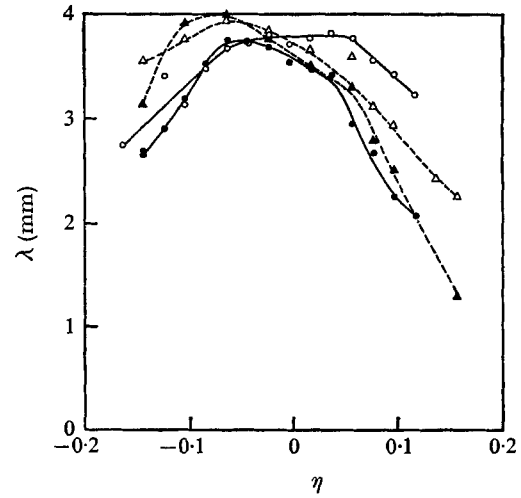

FIGURE 36. The distribution of microscales across the flow (conventional and turbulent zone results). —○—, λf; —●—, $(\lambda f)_T$; --△--, λg; --▲--, $(\lambda g)_T$.

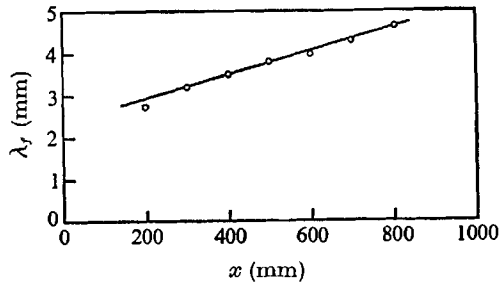

FIGURE 37. The growth of the longitudinal microscale with downstream distance ($\eta = 0$).

9. The energy balance

The equation representing the turbulent energy balance in a two-dimensional flow may be written in the form

$$\underbrace{\left[\frac{\overline{u'v'}}{U_m^2}\frac{\partial}{\partial\eta}\left(\frac{\bar{U}}{U_m}\right)-\eta\frac{\partial}{\partial\eta}\left(\frac{\bar{U}}{U_m}\right)\left(\frac{\overline{u'^2}}{U_m^2}-\frac{\overline{v'^2}}{U_m^2}\right)\right]}_{\text{Production}}+\underbrace{\left[\frac{1}{2}\frac{\partial}{\partial n}\left(\frac{\overline{q^2}}{U_m^2}\right)\left(\frac{\bar{V}}{U_m}-\frac{\bar{U}}{U_m}\right)\right]}_{\text{Convection}}$$

$$\underbrace{\left[+\frac{1}{2}\frac{\partial}{\partial\eta}\left(\frac{\overline{v'q^2}}{U_m^3}\right)-\frac{1}{2}\eta\frac{\partial}{\partial\eta}\left(\frac{\overline{u'q^2}}{U_m^3}\right)\right]}_{\text{Diffusion}}-\underbrace{\left[\eta\frac{\partial}{\partial\eta}\left(\frac{\overline{p'u'}}{\rho U_m^3}\right)-\frac{\partial}{\partial\eta}\left(\frac{\overline{p'v'}}{\rho U_m^3}\right)\right]}_{\text{Pressure transport}}$$

$$=-\frac{x\nu}{U_m^3}\underbrace{\left[\overline{\left(\frac{\partial u'}{\partial x}\right)^2}+\overline{\left(\frac{\partial u'}{\partial y}\right)^2}+\overline{\left(\frac{\partial u'}{\partial z}\right)^2}+\overline{\left(\frac{\partial v'}{\partial x}\right)^2}+\overline{\left(\frac{\partial v'}{\partial y}\right)^2}+\overline{\left(\frac{\partial v'}{\partial z}\right)^2}+\overline{\left(\frac{\partial w'}{\partial x}\right)^2}+\overline{\left(\frac{\partial w'}{\partial y}\right)^2}+\overline{\left(\frac{\partial w'}{\partial z}\right)^2}\right]}_{\text{Dissipation}}.$$

This equation is obtained by applying the boundary-layer approximation to the mean velocity and dropping the viscous diffusion term. Experimental evidence justified these omissions; however, other terms which are often omitted in the literature (like the production resulting from normal stresses) were retained since their contribution was not entirely negligible. The production, convection and diffusion terms were calculated directly from the measured quantities without resorting to further assumptions. The dissipation term was calculated by assuming that

$$\overline{(\partial v'/\partial y)^2}\approx\overline{(\partial v'/\partial z)^2}\approx\overline{(\partial w'/\partial y)^2}\approx\overline{(\partial w'/\partial z)^2}\approx\overline{(\partial w'/\partial x)^2};$$

in fact the dissipation term is practically equal to 9 $\overline{(\partial u'/\partial x)^2}$. This differs from the isotropic case for which the dissipation term is equal to 15 $\overline{(\partial u'/\partial x)^2}$. The pressure transport term is obtained from the above equation. Each term in the energy balance is plotted in figure 38; the conventional measurements are shown as solid lines while the measurements in the turbulent zone are represented by the dashed lines.

The inherent asymmetry in this flow is responsible for a somewhat different appearance of the turbulent energy balance as compared with the balance in the self-preserving axisymmetric jet or wake. For example, the peak in the production which corresponds approximately to the point of inflexion of the mean

velocity profile almost coincides with the place where the dissipation reaches its maximum. The convection and pressure transport terms are negligible on the outer (lower-velocity) side of the mixing region. The convection term, in particular, reaches its maximum at the inner edge of the mixing layer ($\overline{U} \approx 0{\cdot}97U_m$)

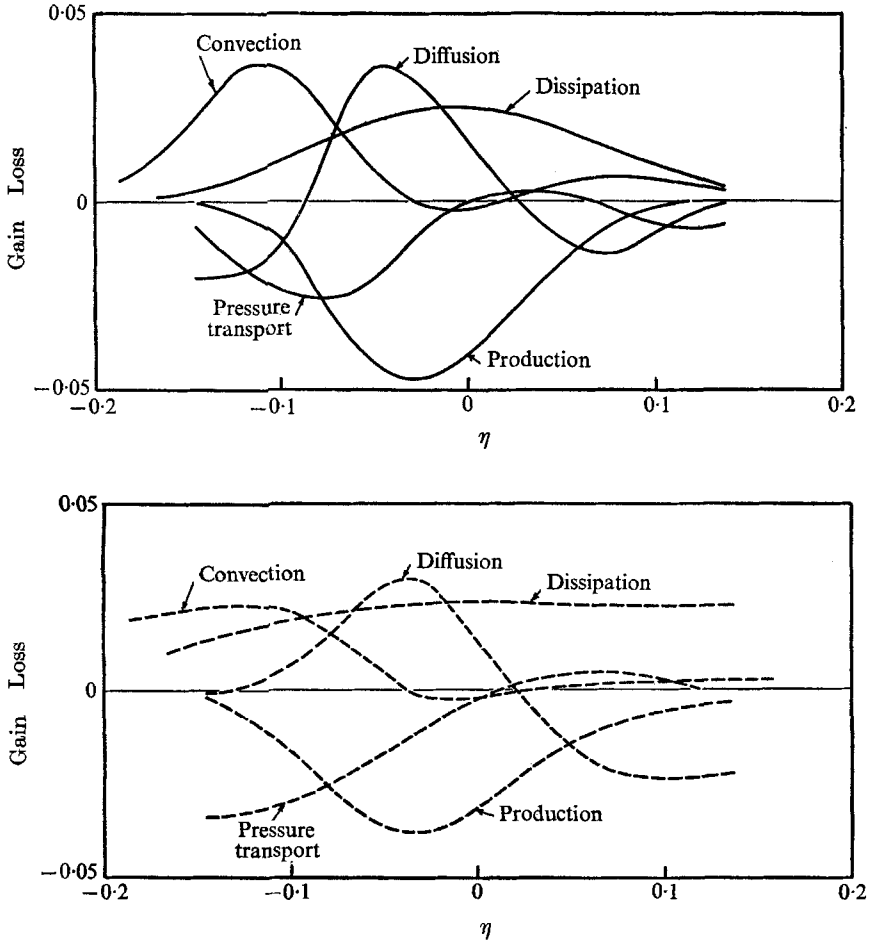

FIGURE 38. The energy balance (conventional and turbulent zone results).

where the turbulent intensity is already quite small. The diffusion term is almost symmetrical about $\eta = -0{\cdot}045$ (where $\overline{v'^2}$ has a peak) and is negative at both edges of the flow.

The balance of energy in the turbulent zone of the mixing region was calculated from the zone average measurements. The dissipation term is not, however, equal to 9 $(\overline{\partial u'/\partial x})^2$ since the three derivatives of the longitudinal fluctuations did not resemble the derivatives of the lateral and transverse fluctuations (figure 35). The spatial gradients of each term in the zone-average balance are less steep than the corresponding terms obtained by the standard method.

The dissipation term in particular is almost invariant across the flow. A detailed comparison between figure 38(*a*) and figure 38(*b*) reveals a number of things: (1) The diffusion term is no longer symmetrical with respect to η and the turbulent energy is transported by the diffusion process from the centre of the mixing region, where the intensity is highest, outwards to the low mean-velocity region. (2) At the outer edge of the mixing region the turbulent energy gained by diffusion is lost to viscous dissipation since all other modes of transport and production are negligible. The impression conveyed by looking at the conventional measurements is that all terms are small but approximately equal in their magnitude. (3) On the inner side of the mixing region the energy lost by convection is gained by diffusion and pressure transport (figure 38(*a*)). The energy balance in this region is very similar to the balance obtained by Townsend (1949) for the outer part of the wake. The similarity comes as no surprise since this part of the mixing region may well be regarded as the outer part of a wake. On the high velocity side of the turbulent zone (figure 38(*b*)) the loss of energy resulting from convection and dissipation is balanced by the gain of energy *via* the pressure transport. (4) Only in the centre of the flow where $\gamma \to 1$ are figures 38(*a*) and 38(*b*) similar. Here the pressure transport and convection are vanishingly small and the gain of energy by production is balanced by diffusion and dissipation.

10. Some interpretation of the results and general conclusions

It seemed instructive to us to compare the present measurements with some of the early measurements of Townsend (1949*a*, *b*; 1950) which lead to the large-eddy-equilibrium hypothesis. In figure 39 the mean turbulent intensity is shown together with the intensity in the turbulent zone. The gradient of the intensity measured in the turbulent zone is somewhat smaller than the conventional mean gradient but it is comparable to it in magnitude. The turbulent energy in the two-dimensional mixing region is thus far from being homogeneous across the flow. An apparent homogeneity could have been derived by assuming that

$$(\overline{q'^2})_T = \overline{q'^2}/\gamma.$$

This equation is, however, in error since the potential fluctuations deep between the turbulent bulges are of the same order of magnitude as those inside the turbulent zone. Similar results were obtained by Kibens (1968) in the turbulent boundary layer. One may also observe from figure 39 the strong correlation between the lateral rate of transport of turbulent energy ($\overline{v'q^2}$) and the gradient of this energy. Consequently the anomaly of energy transport up the local gradient (Townsend 1949) does not exist. The ever increasing value of $(\overline{u'q^2})_T$ on the outer side of the flow as well as the continuously increasing value of $(\overline{v'q^2})_T$ on the inner side is noticeable. It may be indicative of the way the turbulent energy is spread outwards. On the other side of the mixing region most of the energy is being transported in the axial direction while on the inner side it is transported in the lateral direction. It is plausible to suppose, then, that on the high velocity

side, the turbulent bulges push outwards while they mainly spread in the axial direction on the outer side of the mixing region. The large ratio in magnitude between $(\overline{u'q^2})_T$ at large positive values of η and $(\overline{v'q^2})_T$ at large negative values of η may explain the reason why the mixing region spreads primarily outwards. Indeed if one defines a width of the flow by a constant ratio of turbulent zone mean velocity (say, between the locations at which $(\overline{U}/U_m)_T = 0{\cdot}25$ and $(\overline{U}/U_m)_T = 0{\cdot}75$) one finds that the ratio of the spread of the flow outwards from the step to the spread of the flow inwards is equal to the ratio $(\overline{u'q^2}/\overline{v'q^2})_T$ at these two locations.

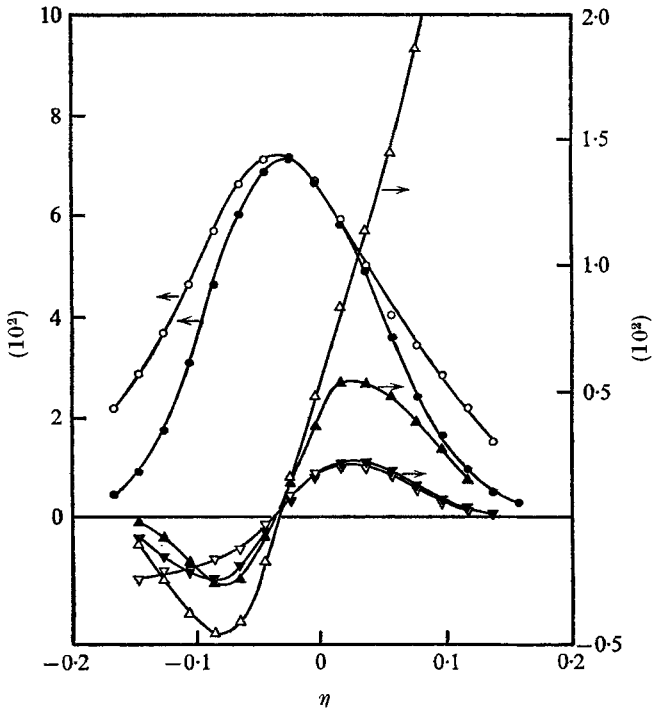

FIGURE 39. The distribution of fluctuation intensities and diffusion terms across the mixing layer (conventional and turbulent zone results). ●, $(\overline{q^2}/\overline{U_m^2})$; ○, $(\overline{q^2}/\overline{U_m^2})_T$; ▲, $(\overline{uq^2}/\overline{U_m^3})$; △, $(\overline{uq^2}/\overline{U_m^3})_T$; ▼, $(\overline{vq^2}/\overline{U_m^3})$; ▽, $(\overline{vq^2}/\overline{U_m^3})_T$.

The turbulent momentum exchange coefficient (eddy viscosity) and energy exchange coefficient (eddy diffusivity) are plotted in figure 40. The eddy viscosity when measured in the turbulent zone is fairly constant across the entire flow. The energy exchange coefficient is much more scattered but it too may be considered as constant. At any rate $(\overline{v'q^2})_T$ seems to depend on the gradient of the turbulent intensity and is not very different in magnitude from the eddy viscosity.

The various averages of the lateral mean velocity are shown in figure 41 together with the bulk convection velocity $(\overline{v'q^2}/\overline{q^2})$. The measurements were

made with an X wire and thus the absolute magnitude of the results should be treated with some reservation. The experimental procedure was as follows. The response of the wires was linearized and matched as close as possible. However, this procedure could at best be accurate to within 1 % which could cause an error of more than 100 % in $\overline{V}$. Consequently the probe was moved to a position $\eta \approx -0{\cdot}02$ where $\overline{V}$ was calculated to be 0·011 and the lateral velocity as measured there on the first such trial was 0·019. A small adjustment in the amplification of one of the signals yielded finally the expected result. The probe was then removed from the mixing region, the response of each wire to changes in axial velocity was rechecked and, when found essentially identical to the previous calibration, measurements of $\overline{V}$ proceeded.

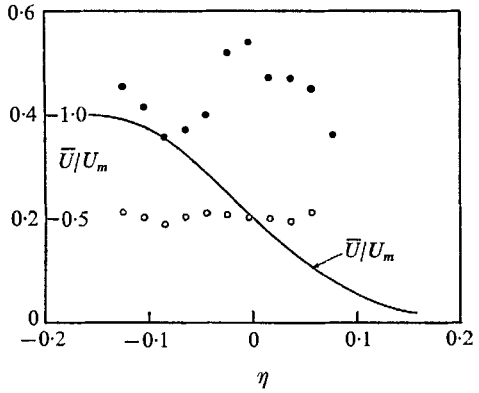

FIGURE 40. The eddy viscosity and eddy diffusivity in the turbulent zone. ○, $\left[\overline{\frac{u'v'}{U_m^2}}\Big/\frac{d'}{d\eta}\left(\frac{\overline{U}}{U_m}\right)\right]_T \times 10^2$; ●, $\left[\overline{\frac{v'q^2}{U_m^3}}\Big/\frac{d}{d\eta}\left(\frac{\overline{q^2}}{U_m^2}\right)\right] \times 10^2$.

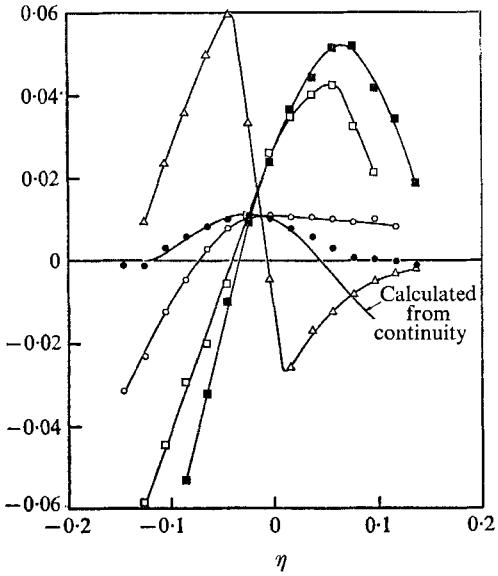

FIGURE 41. The comparison between mean lateral velocities and bulk convection velocities. ●, $\overline{V}/U_m$; ○, $(\overline{V}/U_m)_T$; △, $(\overline{V}/U_m)_p$; ■, $(\overline{v'q^2}/U_m\overline{q^2})$; □, $(\overline{v'q^2}/U_m\overline{q^2})_T$.

The direction of $\overline{V}_T$ at both edges of the flow is outwards, but while the magnitude of $\overline{V}_T$ is almost constant on the low-velocity side it increases with lateral distance on the high-velocity side. The ratio between magnitudes of $\overline{V}_T$ on both sides of the flow strengthens the argument presented in the previous section about the different mechanism in which turbulent energy is being diffused outwards. The bulk convection velocity which is also shown on this figure appears to be anomalously high at most places across the flow. Although Townsend (1956) explained the disparity between $\overline{V}_T$ and $(\overline{v'q^2}/\overline{q^2})$ the same argument no longer applied with respect to $(\overline{v'q^2}/\overline{q^2})_T$. The disparity between $\overline{V}_T$ and $(\overline{vq^2}/\overline{q^2})_T$ or $(\overline{v'q^2}/\overline{q^2})$ is large; larger than the disparity between corresponding quantities in the wake (Townsend 1956). Furthermore, on the inner side of the flow the two curves diverge from one another as the distance from the centre increases.

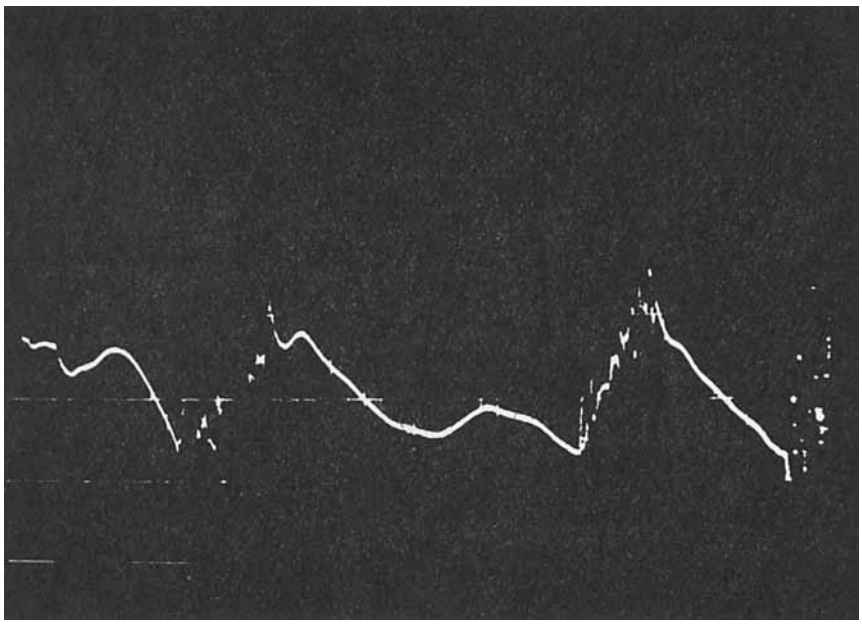

FIGURE 42. An oscillogram of the trace of the lateral velocity. (Amplification: 1 cm = 0·125 U_m. Time scale: 1 cm = 10 msec.) Position: $\eta = -0{\cdot}11$.

One may define a characteristic ratio between lateral and longitudinal time scales as

$$(l_0/\overline{V}_T)/(x/\overline{U}) \approx 6,$$

where l_0 is the half width of the flow; $\overline{U}, V_T$ are here representative mean velocities. The fact that this number is larger than unity implies that on the average the entire flow attains its equilibrium in a shorter time than it takes a packet of fluid to travel across the flow, unless such a packet makes the trip several times in a more or less regular manner. Continuous observations of the trace of the lateral velocity, V, revealed such regularity within the turbulent zone. It is apparent from figure 42 that $\overline{V}_T$ varies almost linearly with time and the values of $\overline{V}_T$ at which the probe enters or leaves the turbulent front seem to be quite constant. (The

constant varies from point to point with the flow). It may be suggested that the large eddies rotate like a solid body and thus as long as they remain large they contribute little to the lateral transfer of turbulent energy. The possible solid-body rotation of the large eddies is quite appealing as it may also explain the linear spatial distribution of the point-average axial velocity profiles. The idea of jets shooting out from the core of the turbulent fluid is unlikely because nowhere did V_T have a jet-like profile. It appears, however, that the instantaneous lateral velocity may reach as much as 10 % of the axial velocity in this flow (figure 42). The point average measurements of Kibens (1968) indicated that the lateral velocity in the boundary layer did not exceed 1·5 % U_∞, thus the presence of the wall may have a strong inhibiting effect on the size and strength of the large eddies. One may conclude that $\overline{V_T}$ carries rather little information about the mechanism of lateral energy transport. Point averages without time delay will only give the extreme values of V whenever the probe enters or leaves the turbulent zone. To obtain more complete information one should sample the V_T signal at various time delays after the probe enters the turbulent front. At any rate, the transfer of energy or momentum down the intensity gradient cannot be ignored.

Phillips (1967) compared his calculations of the maintenance of Reynolds stresses in turbulent shear flow with the measurements of Liepmann & Laufer (1947) and supplemented them with the data of Davies *et al.* (1963). Since all necessary quantities were essentially measured in the present investigation another comparison seemed in order. First, the integral time scale in the moving frame was obtained by assuming $R_{11\tau}$ to have a simple exponential form (see also Davies *et al.*). The procedure is not accurate because these correlation measurements did not extend below 0·5 but the same procedure was also applied by Davies *et al.* The results are tabulated below:

η	$\frac{U_m}{x}$	$\frac{d(V/U_m)}{d\eta}$	$\left[\frac{d(V/U_m)}{d\eta}\right]_T$	A	A_T
−0·1	0·55	2·5	2·80	0·265	0·236
−0·05	0·55	4·6	4·00	0·199	0·218
0	0·652	4·7	3·95	0·188	0·206
0·05	0·885	3·7	2·80	0·204	0·240
0·1	1·03	2·4	1·45	0·202	0·600

The value of A was derived from the equation

$$\frac{\overline{u'v'}}{U_m^2} \simeq A \frac{\overline{v'^2}}{U_m^2} \frac{\Theta U_m}{x} \frac{d(V/U_m)}{d\eta},$$

where the values of the shear stress and the intensity of the lateral fluctuations is given in figures 14 and 18. The results are rather encouraging, particularly if one keeps in mind the manner in which Θ was evaluated. The value of A varies rather little across the flow and may be assumed to be equal to 0·2. The calculations based on previous data yield $A = 0{\cdot}17$.† The corresponding results for A in the

† Phillips calculated the constant from the equation $\Theta(dU/dy) \simeq 3{\cdot}2$ but there is a corrigendum to the paper of Davies *et al.* stating that $\Theta(dU/dy) \approx 4{\cdot}5$.

turbulent zone vary more across the flow. The integral scale in the moving frame did not seem to be correlated with the gradient of the mean velocity as it was in the observations of Davies *et al.*

The following conclusions may be drawn from this investigation: (1) The turbulent part of the mixing layer can be divided into two zones one on the high velocity side and one on the low velocity side. (2) The two interfaces binding the mixing layer move independently of each other.† (3) The exponential velocity profile does not exist instantaneously in this case. (4) The turbulence in this flow is not subjected to a constant mean shear because $\langle dU/d\eta \rangle$ oscillates depending on the location of the interface. (5) The turbulence is not homogeneous and is in general non-isotropic. (6) The simple constant eddy viscosity and eddy diffusivity concepts apply remarkably well to the turbulent zone of this flow. (7) The measurements in the turbulent zone are probably more accurate than the conventional measurements.

The authors are indebted to Mr F. Lange who constructed all the non-standard electronic equipment. They also wish to express their appreciation to Professors J. Laufer and L. S. G. Kovasznay for their interest and stimulating discussions.

Part of the work by the first author was done while on sabbatical leave at the Technion-Israel Institute of Technology.

REFERENCES

Bradbury, L. J. S. 1965 *J. Fluid Mech.* **23**, 31.

Bradshaw, P. 1967 *J. Fluid Mech.* **27**, 209.

Bradshaw, P., Ferris, D. H. & Johnson, R. F. 1963 *NPL Aero Rep.* 1054.

Champagne, F. H. & Sleicher, C. A. 1967 *J. Fluid Mech.* **28**, 177.

Corrsin, S. & Kistler, A. L. 1955 *NACA Rep.* 1244.

Davies, P. O. A. L., Fisher, M. J. & Barratt, M. J. 1963 *J. Fluid Mech.* **15**, 337.

Demetriades, A. 1968 *J. Fluid Mech.* **34**, 465.

Heskestad, G. 1965 *J. App. Mech.* **32**, 721.

Hwang, N. H. C. & Baldwin, L. V. 1966 *J. Basic Engng.* **88**, 261.

Kibens, V. 1968 Doctoral Dissertation, Johns Hopkins University.

Klebanoff, L. L. 1955 *NACA Rep.* 1247.

Laurence, J. C. 1956 *NACA Rep.* 1292.

Liepmann, H. W. & Laufer, J. 1947 *NACA Tech. Note*, 1257.

Phillips, O. M. 1955 *Proc. Camb. Phil. Soc.* **51**, 270.

Phillips, O. M. 1967 *J. Fluid Mech.* **27**, 131.

Townsend, A. A. 1949*a* *Proc. Roy. Soc.* A **197**, 124.

Townsend, A. A. 1949*b* *Aust. J. Sci. Res.* **2**, 451.

Townsend, A. A. 1950 *Phil. Mag.* **41**, 890.

Townsend, A. A. 1951 *Proc. Camb. Phil. Soc.* **47**, 375.

Townsend, A. A. 1956 *The Structures of Turbulent Shear Flow.* Cambridge University Press.

Wygnanski, I. & Fiedler, H. E. 1969 *J. Fluid Mech.* **38**, 577.

† While this paper was in press a more direct measurement, confirming this result in a similar flow, was made.